Poly: A Perfect Storm - Phenomenology, North Sea Influence, and Insights into Hybrid Cyclogenesis

A. Kees - 1230123

Supervisors: M. Baatsen, H. de Vries and N. Bloemendaal

IMAU, Utrecht University

Department Research and Development of Weather and Climate models, Royal Netherlands Meteorological Institute (KNMI)

July 2024

Abstract

Windstorm Poly, which developed overnight from 4th to 5th, 2023, was a major summer windstorm in the Netherlands, characterized by rapid intensification and severe wind gusts. The Royal Netherlands Meteorological Institute (KNMI) issued severe weather warnings, including code red, as the storm's windfield intensified. The storm resulted in wind gusts of up to 146 km/h in IJmuiden and significant damage from Zandvoort to Alkmaar. This study investigates the development and unique characteristics of Storm Poly, focusing on the influence of record-high sea surface temperatures and atmospheric dynamics. We use the Regional Atmospheric Climate Model (RACMO), Harmonie and ERA5 reanalysis data to analyze Poly's formation and evolution. Our findings suggest that the interaction between an upper-level trough and convective showers was the primary driver of the storm's rapid intensification. The RACMO simulations demonstrate that while Sea Surface Temperatures (SSTs) variations impacted the storm's characteristics, including wind speed, precipitation, and storm scale, they are not the dominant factor in Poly's rapid cyclogenesis. The study also explores the hypothesis of a sting-jet phenomenon contributing to Poly's severe wind gusts. However, analyses from ERA5 and the new cycle of HARMONIE (CY46) datasets showed no evidence of typical sting-jet dynamics. Instead, the strongest winds are attributed to surface processes and warm-core dynamics, indicative of a hybrid cyclone undergoing subtropical transition. This research highlights the complexity of storm dynamics and underscores the need for improved high-resolution modeling to understand and predict similar events. Future investigations should focus on past severe summer storms in the Netherlands to determine if Storm Poly is unique in its hybrid characteristics and consider the implications of climate change on the future frequency and intensity of such storms.

Acknowledgements

I would like to wholeheartedly thank my supervisors, Michiel Baatsen (University of Utrecht), Hylke de Vries (KNMI), and Nadia Bloemendaal (KNMI), for their expert supervision during the past year. Their support has been integral to my success and enjoyment of my internship at KNMI, and I feel incredibly fortunate to have had this experience.

I would also like to extend my thanks to the meteorologists at KNMI: Yorick de Wijs, Thom Zwagers, and Rob Groenland, for their expert input and cooperation during my research.

Additionally, I am very grateful to my in-laws for providing the availability of their 'prieeltje' in their garden, where I could work on my thesis every weekend

And, of course, I would like to thank Marjolein Ribberink as a friend for making the KNMI experience even more enjoyable through our mutual excitement about storms and the climate, and for her help when things were not going as smoothly.

Thank you all for making this journey an educational and rewarding one.

Contents

1 Introduction

Windstorm Poly, a substantial summer windstorm, developed overnight from 4th to 5th July, 2023. The Royal Netherlands Meteorological Institute (KNMI) issued code orange, followed by code red, which is the highest possible weather alarm in the Netherlands, because of the worrying intensification of the windfield. At peak intensity wind gusts of 146 km/h were recorded in IJmuiden, along with an hourly average windspeed of 108 km/h (11 Beaufort) for two consecutive hours. The greatest impact was reported in a narrow area from Zandvoort to Alkmaar, causing one fatality and serious injuries to several individuals due to fallen trees. The extensive damage was largely due to the fully foliaged trees, heightening their risk of being uprooted or branches breaking. The event also led to significant transportation disruptions, including overturned trucks, a derailed tram, suspended train services, and the cancellation of over 400 flights at Schiphol Airport. Additionally, several highways were closed and rendered impassable. Financial losses are a combined €50 billion over the United Kingdom, Belgium, Germany and the Netherlands.

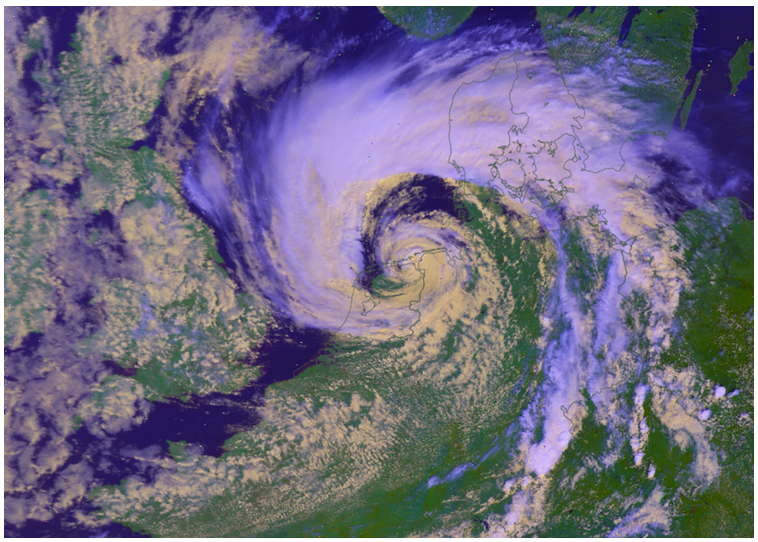

Figure 1: Satellite image composite of Poly on 5th July 2023 0730 UTC. Source: Sentinel 5P, European Space Agency

Poly proved to be an unusual summer windstorm, sparked by the interaction between a deepening upper-level trough and a small convective layer above Brittany, leading to rapid cyclogenesis (RACY) or bombogenesis. The storm was notable for its distinct 'perfect curl' (Fig.1), with intense winds and precipitation wrapping around the cyclone's warm and dry core, also known as the dry-slot, resulting in a comma-shaped cloud pattern. This pattern is a key characteristic of the Shapiro-Keyser (SK) conceptual model which describes the structure and evolution of extratropical cyclones (ETCs) (Shapiro & Keyser, 1990). The lowest sea level pressure was recorded in De Kooy, on the North coast of Noord-Holland, at 988 hPa (no pressure data was available in IJmuiden), although it is believed that the storm's peak intensity reached even lower pressure minima. Wind gusts exceeded 100 km/h at ten weather stations, peaking at 146 km/h in IJmuiden at 0700 UTC (09:00 local time), right during rush hour.

This categorizes Poly as the 7th most intense summer windstorm by KNMI's criteria based on the storm number, and potentially ranking in the top three based on the largest 25% of wind gusts observed. However, due to the rare occurrence of summer storms in the Netherlands, KNMI struggles with the definition of summer storms as it includes all storms during April through September. One could argue that this definition does not differentiate between early- or late autumn/winter storms and summer storms based on climatology. On top of that, meteorological autumn starts on the first of September. Consequently, KNMI also refers to some of these September storms as 'autumn storms' when they are mentioned somewhere else. Table 1 illustrates why Storm Poly was truly an exceptional event compared to other summer storms. It is the only

time that 11 Bft was recorded during summer, and the peak gusts were substantially higher than those of any other summer storm in the Netherlands.

Rank	Date	Windspeed (Bft)	Windspeed (km/h)	Max. windgust (km/h)
1	28 May 2000	10	90	130
2	12 May 1983	9	85	131
5	25 July 2015	10	90	122
6	14 August 1985	6	48	124
7	5 July 2023 - Poly	11	108	146

Table 1: Top 7 strongest summer storms in the Netherlands since 1970 based on storm number. Windspeed is the maximum hourly average windspeed recorded in the Netherlands. Note that we excluded storms that occurred in September.

Meteorologist at KNMI were surprised about Poly's development and intensity as well. Earlier model runs on 3 and 4 July indicated that most activity would be concentrated over the northeast of the Netherlands and the German Bight. However, the development of the low-pressure area shifted progressively westward, resulting in the heaviest wind gusts also moving further west and intensifying. Initially, forecasts emphasized significant precipitation amounts, but as the event drew closer, the importance of wind conditions increased substantially. On the evening of 4 July, KNMI initially issued a code yellow warning. However, due to rapidly evolving conditions, they had to urgently escalate the weather warnings overnight. Code orange was issued by KNMI just after 0200 UTC on 5 July for the provinces Zuid-Holland, Noord-Holland, Flevoland, the IJsselmeer-area, the Wadden-area, Friesland, Overijssel, Drenthe, and Groningen. Due to the storm's intensification and subsequent display of Sting-Jet (SJ) characteristics, KNMI escalated to code red at 0530 UTC for the provinces of Noord-Holland, Flevoland, the IJsselmeer area, and Friesland. By 1300 UTC, the code orange weather alert had been lifted for all provinces. However, code yellow remained in effect for the provinces of Groningen, Friesland, and Drenthe due to the potential for severe wind gusts. The overnight escalation from code yellow to code red is an indication of the astonishment that meteorologists experienced in the weather room at KNMI. Meteorologists explained that Poly displayed behaviour that did not match their knowledge and previous experience with summer windstorms. One meteorologist even dubbed Poly "a freak storm" (de Wijs, Y., Zwagers, T. and Groenland, R., personal communication, 13 February, 2024).

Poly's 'freak' behaviour did not go unnoticed by the media, as multiple news outlets, including interviews by local experts, speculated about the storms cause. Extreme weather phenomena like this one are often immediately linked to climate change and Poly was no exception. June 2023 was the hottest on record since 1901 with an average temperature of 19.4°C compared to 16.4°C as the normal average. Additionally, global sea surface temperatures (SSTs) were at an all time high since April 2023 and the North Atlantic SST was 1°C above average as well (Huang et al., 2021). So it is unsurprising that the link with climate change was quickly made. The narrow strip of intense winds was also subject to speculation. This destructive feature of the storm was hypothesized to be a SJ, a rare phenomenon producing high-speed, downward-moving dry air from a warm, dry intrusion. However, this explanation is not so straight-forward as the 'SJ' was located at an odd location which we will discuss later.

How climate change could impact the frequency, development and intensity of storms has been a subject of research for some time. Precipitation and wind velocities during storms are anticipated to rise in a warming climate (Bui & Spengler, 2021; Sinclair et al., 2020). ETCs are the most common over Western Europe and they are purely driven by baroclinicity. They occur most frequently during the winter months when the temperature difference between the equator and the midlatitudes is greatest. Storm tracks in the mid-latitudes could intensify, expand and shift poleward due to the enhanced energy imbalance between the Northern and Southern Hemisphere due to climate change. Areas of maximum baroclinicity might intensify and could shift poleward and this shift leads to an increase in eddy transport of latent heat to balance the enhanced meridional gradient of the planetary energy balance. However, the precise location of the storm tracks are quite variable so the exact impact of this is uncertain (Seneviratne et al., 2021; Tamarin-Brodsky & Kaspi, 2017; Wu et al., 2011). Although frequency and storm intensity are commonly linked

to climate change, a somewhat underexposed subject is the change in nature of storms. Storm formation occurs in widely different climatic conditions, where tropical cyclones (TCs) are commonly found just off of the equator, polar lows cause havoc over the poles. And there is a whole range in between: warm-seclusion cyclones, subtropical cyclones (SCs), ETCs, hybrid cyclones and remnants of TCs. Due to climate change, there is a shift in the development of certain types of cyclones. For example, twenty-first century TCs are likely to occur over a wider range of latitudes (Dekker et al., 2018; Studholme et al., 2022).

Poly deviates from the expected behaviour of a normal ETC with its rapid development, 'perfect curl' and compact but intense windfield which is located right beside the frontal precipitation band. These characteristics are typically observed in (sub-)tropical cyclones and suggest a strong connection to surface fluxes (Wood et al., 2023). It has been ascertained that the surface latent heat fluxes associated with the absolute SST are critical for moist baroclinic development. Elevated SSTs lead to increased surface latent heat fluxes, thereby enhancing diabatic heating around a cyclone's core (de Vries et al., 2019; Quitián-Hernández et al., 2020). Bui and Spengler (2021) demonstrated that the absolute SST in the 24 hours preceding a cyclone's peak intensity critically influences its deepening. Furthermore, they discovered that cyclones undergo explosive development when the SSTs ahead of the storms exceed 16.8°C prior to their intensification phase. SSTs also have a direct impact on SC formation and intensity over the Mediterranean Sea (also known as medicanes) (Varlas et al., 2023). SC Alpha (2020) is also believed to have transitioned from an ETC to a SC of the coast of Portugal due to the temperature difference between the SST and the temperature at 500 hPa, which was around 34°C - 37°C at the time (Berg, 2021). This highlights the significant role of SST in cyclonic development and intensity, and it shows the need for further investigation into the mechanisms driving Poly's unusual intensity and its connection to the SST anomalies.

As mentioned before, the narrow strip in North Holland where the highest wind gusts occurred puzzled meteorologists. This localized swath of intense wind gusts alluded to the presence of a SJ; however, the manifestation of such extreme gusts within the storm's structure challenges traditional SJ characteristics which is usually found at the occluding front's tail end. Instead, Poly's severe gusts were located anomalously, on the inner side of the cold conveyor belt (CCB). This atypical placement adds complexity to the storm's analysis and raises questions about the conventional understanding of SJ dynamics in relation to the storm's path and intensity. To explain the peculiarities of Poly's wind pattern in the context of its rapid development and the influence of the North Sea's warm waters we propose three main research questions:

1. What are the unique characteristics and development mechanisms of Storm Poly within the current climatic context.

2. How does Poly evolve under altered climatic conditions (warmer and cooler).

3. What is the impact of the anomalously high SSTs of the North Sea on Storm Poly's development within the current climate.

We review literature and analyze available reanalysis data (ERA5 and HARMONIE) and Numerical Weather Prediction (NWP) forecasts to unravel Poly's development and characteristics. We also employ dynamical down-scaling techniques to simulate Poly within current and varied climate scenarios using the Pseudo Global Warming (PGW) approach with the Regional Atmospheric Climate Model (RACMO). And to assess the impact of unprecedented SSTs on Storm Poly's formation, this study analyzes RACMO model simulations adding uniform SST perturbation ranging from -4°C to +4°C, with one degree increments.

2 Methodology

2.1 Data and Model Specifications

The datasets used for this study are the 0.25°-resolution ERA5 reanalysis dataset (Hersbach et al., 2020) and the newest version of Harmonie, Cycle 46 UVMix off (CY46) at 2.5 km resolution initialized at 5 July 00 UTC. These datasets facilitate the detailed examination of the physical atmospheric processes within Storm Poly. Key questions include: identifying the factors contributing to Poly's rapid intensification, such as the potential roles of SJs and convection processes, and the methodologies to detect these mechanisms within the data. Incorporating insights from discussions with NWP forecasters will also contribute to the evidence base regarding SJ phenomena and Poly's phenomenology.

To simulate Poly in a different climate we use RACMO. A quasi-operational RACMO mini PGW-ensemble is created by running RACMO in forecast mode, using four different initial conditions and boundaries from the European Centre for Medium-Range Weather Forecasts' (ECMWF) operational model. A set of 'future weather' runs is then created by adding a PGW perturbation at the boundaries of the regional model (Brogli et al., 2023; Schär et al., 1996). In the interior, the regional model adapts to these modified boundary conditions, capturing what is believed to be a significant portion of the thermodynamic adjustment to global warming. It is crucial to balance starting the simulation early enough to allow for these adjustments, while also starting late enough to ensure the circulation remains similar to the control simulation. The situation with Storm Poly is particularly delicate, as even minor imposed changes in circulation could lead to tracks over land, resulting in the dissipation of Poly. The delta fields that are added at the boundaries of the PGW simulation (and initial conditions) are derived for a +3°C warmer world (compared to a reference of 1991-2020), using the dry11 and wet11 subset of CMIP6 models used in the KNMI'23 scenario's. Additionally, we set up a +1.5°C warmer and a -1.5°C cooler climate run. For each warming/cooling level, this results in 2 x 4 members (CTL and FUT), each with a duration of 72 hours. The output, provided hourly on pressure levels, has a 12 km resolution and is regridded to a longitude-latitude grid.

However, as will be discussed later in section 3.4, the PGW simulations did not yield any particularly useful results partly due to the initial conditions under which the model was run. To investigate this further, we examine the RACMO HindCast (HC) runs, which commence every six hours and are initialized with the ECMWF operational analysis, starting on 3 July at 0000 UTC. Every six hours, the lateral boundary conditions are forced by the ECMWF analysis, and the data is interpolated from this input. The findings from this analysis, which are discussed in detail later, prompts the initiation of a new experiment that we initiate on 4 July at 1200 UTC. In this new approach, RACMO is run with modified SST scenarios, where the SST is uniformly adjusted in intervals of 1°C, ranging from -4°C to +4°C. This methodology aims to isolate the impact of the anomalously warm North Sea.

We evaluate the performance of RACMO by comparing several characteristics of windstorm Poly in the current climate run with observations and the CY46 model output. We will investigate changes in precipitation, wind speed (maxima), minimum sea level pressure, intensification, storm track and (geometric) vertical velocities. Observations are obtained from two of KNMI's weather stations; IJmuiden and De Kooy (Den Helder) (Source: KNMI).

2.2 Tracking Poly

We (back-)track Storm Poly through the point of minimum mean sea level pressure (MSLP). In this thesis, we utilize different datasets, each presenting Poly with varying points of origin and intensity. To address this, we track Poly in every run starting from 6 July, 0000 UTC, when it is a fully developed storm. From this point, we identify its location in the previous hour by finding the minimum MSLP within a box with sides of 1.5° longitude and latitude around the initial point. This method allows us to follow Poly back in time and accurately determine the point of origin according to each dataset.

2.3 Sting-Jet diagnostic

According to Clark and Gray (2018) a SJ is defined as "a coherent airflow that descends from mid-levels inside the cloud head into the frontal-fracture region of a SK cyclone over a few hours, leading to a distinct region of near-surface stronger winds." This process occurs above the CCB during some stage of its lifecycle and, in some cases, descends to reach the top of the boundary layer ahead of the CCB. The term SJ hints at its common location, resembling the sting at a bent-back occlusion's end, often likened to a scorpion's curved tail. SJs are identified in satellite imagery by developing cloud bands with dark bands between them, in infrared imagery of the cloud head, and observations of surface rainfall, combined with a narrow band of enhanced surface wind gusts (Browning, 2004).

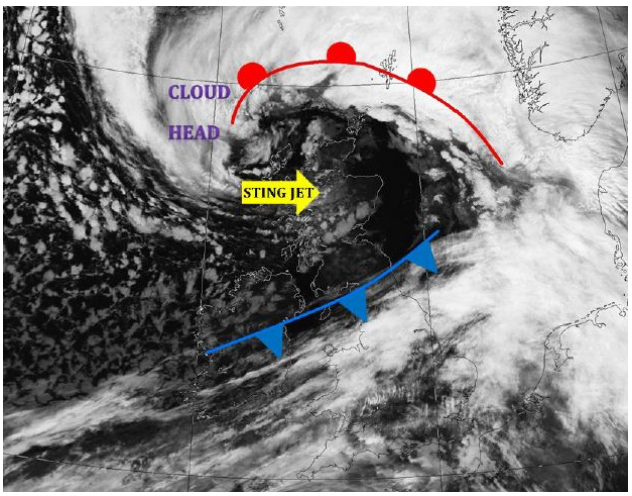

Figure 2: Satellite image of a developing extratropical cyclone, highlighting key features: the warm front (marked by red dots), a potential sting jet visible as the dark band protruding from the cloud head(yellow arrow), and the cold front (blue triangles). From the Royal Meteorological Society.

To confirm the presence of a SJ and ensure the enhanced surface wind is not due to the CCB or other ETC feature, analysis of model (reanalysis) data is necessary. The identification of a SJ in this study follows the diagnostic presented by Manning et al. (2022, 2023), focusing on three SJ characteristics: the slantwise descent, a reduction in relative humidity (RH) in the cloud head, and high wind speeds in front of the cloud head. The slantwise descent is noted by a reversal in the vertical gradient of horizontal wind speed at 600 hPa, 700 hPa, 800 hPa and 900 hPa (Manning et al., 2023). This descent is from an area of high RH ($\rangle$80%) at 500 hPa to an area of low RH ($\langle$50%), with a significant drop in RH ($\rangle$80%), illustrating the movement from the moist cloud head into the dry slot. Furthermore, Manning et al. (2022) suggest that for a SJ diagnosis, the maximum wind speed at 850 hPa in the negative wind gradient sequence should be at least 6m/s higher than the maximum speed in the positive area.

Streamlines are manually identified by analyzing wind speed streamplots (Matplotlib.pyplot.streamplot()) at 850hPa combined with RH at 500hPa at specific times. Regions exhibiting the highest wind speeds, especially those proximate or directly over the bent-back occlusion, are examined for potential SJ activity. In this process, streamlines are carefully extracted over these areas of interest, with four specific streamlines chosen for the detailed analysis under discussion. This methodology is employed not only for the analysis of Storm Poly (0700 UTC 05-07-23) but also for Storm Ciarán (1700 UTC 01-11-23). Storm Ciarán was a significant windstorm impacting western Europe from late October to early November 2023, exhibited evident SJ signatures in both satellite and radar data. Consequently, this storm serves as an illustrative case study for the manifestation of SJs within the ERA5 reanalysis framework, enhancing our understanding of their characteristics and detection in reanalyzed atmospheric datasets.

2.4 Hart diagram

To analyze the structure and evolution of Storm Poly, we employ the phase-space framework proposed by Hart (2003). This is an objective method most commonly used to identify the extratropical transition (ET) of TCs. It examines the lower and upper thermal wind (T_L and T_U in m/s) of the cyclone and checks the thermal symmetry of the cyclone. The thermal symmetry parameter, B (m), compares the average 900-600 hPa geopotential thickness over two semicircles with a 500 km radius centered on the cyclone. Low values of B indicate a thermally symmetric or TC, while high values suggest a thermally asymmetric, ETC:

$$B = \overline{Z_{600hPa} - Z_{900hPa}}|_R - \overline{Z_{600hPa} - Z_{900hPa}}|_L \tag{1}$$

keep in mind that the geopotential heights on the right and left semicircles are relative to the cyclone's direction of travel. Values of B below 15 are considered to be indicative of a symmetric storm, such as a TC. This is different than the value proposed by Hart (2003) because a study done by Studholme et al. (2015) found that a value of 10 with higher-resolution data could give false-alarms for ETs and they found a mean B value of 13 for the North Atlantic representative for ET. So, a B value of 15 should be reasonable (Zarzycki et al., 2017). The lower (T_L) and upper (T_U) thermal wind parameters are calculated for the atmospheric layers between 900–600 hPa and 600–300 hPa using the following formula:

$$T_L \equiv -|V_T^L| = \frac{\partial \Delta Z}{\partial \ln p}\bigg|_{900hPa}^{600hPa} \tag{2}$$

$$T_U \equiv -|V_T^U| = \frac{\partial \Delta Z}{\partial \ln p}\bigg|_{600hPa}^{300hPa} \tag{3}$$

where $\Delta Z = Z_{max}$-Z_{min}, p is pressure and Z_{max} and Z_{min} are the highest and lowest geopotential heights at a certain pressure level within a 500 km radius of the cyclone center. The height perturbation (ΔZ) is proportional to the geostrophic wind, and its derivative with respect to pressure effectively measures the scaled thermal wind magnitude. Essentially, positive values of T_L or T_U indicate a warm-core, whereas negative values indicate a cold-core. Warm-core cyclones, such as TCs, form over warm waters. They intensify primarily through wind-driven evaporation and the release of latent heat. These cyclones exhibit a temperature maximum near the center and decay over colder water or land due to the loss of this heat source. Warm-core cyclones are typically characterized by strong convection near their centers and a symmetric structure. Cold-core cyclones, often ETCs, form in mid-latitudes due to temperature gradients and wind shear. They intensify through baroclinic processes and decay as these instabilities are resolved. Cold-core cyclones typically have a temperature minimum near the center and show a more asymmetric structure with fronts (Hart, 2003). Recent studies have shown that cyclones can exhibit characteristics of both warm-core and cold-core structures, especially during transitions such as ET and warm seclusion (where an extratropical cyclone develops a warm core) (Brand & Guard, 1978; Kornegay & Vincent, 1976). These hybrid cyclones blur the lines between the traditional categories, demonstrating the continuum of cyclone structures influenced by both baroclinic and convective processes.

3 Data analysis, results and discussion

3.1 Phenomenology

The radar image at 0300 UTC (Fig.3a) shows a band of precipitation moving from the west towards the Netherlands, with moderate to heavy precipitation indicated by the green and yellow hues. Strong wind patterns are visible, particularly in the northern and coastal areas of the Netherlands. The close proximity of the green and red hues suggests strong horizontal wind shear and possibly rotating winds, which is typical in severe weather systems, but at this stage, the system is not well-organized. This image caused some confusion among meteorologists at KNMI due to the presence of two protrusions in the precipitation, making it unclear where the actual center of the cyclone is located. These protrusions are mesoscale features along a bent-back occlusion, likely rotating around a common but not yet well-defined center.

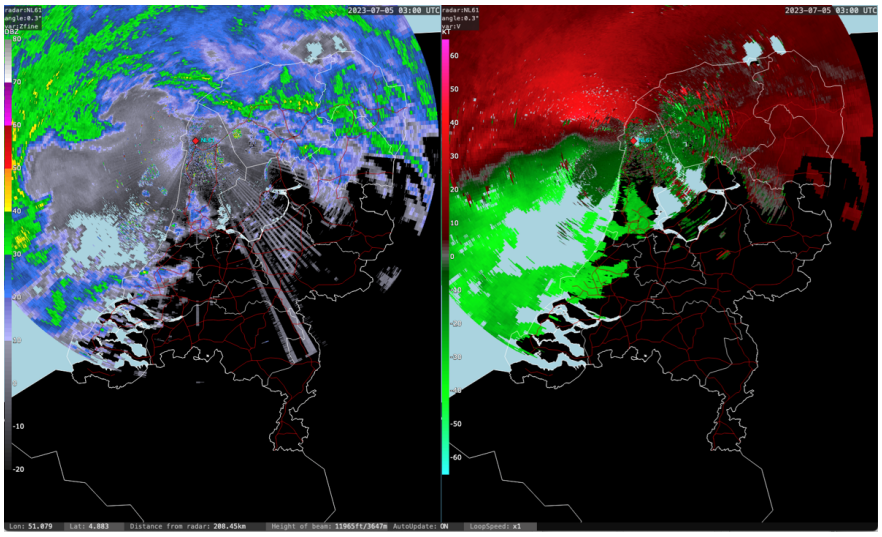

(a)

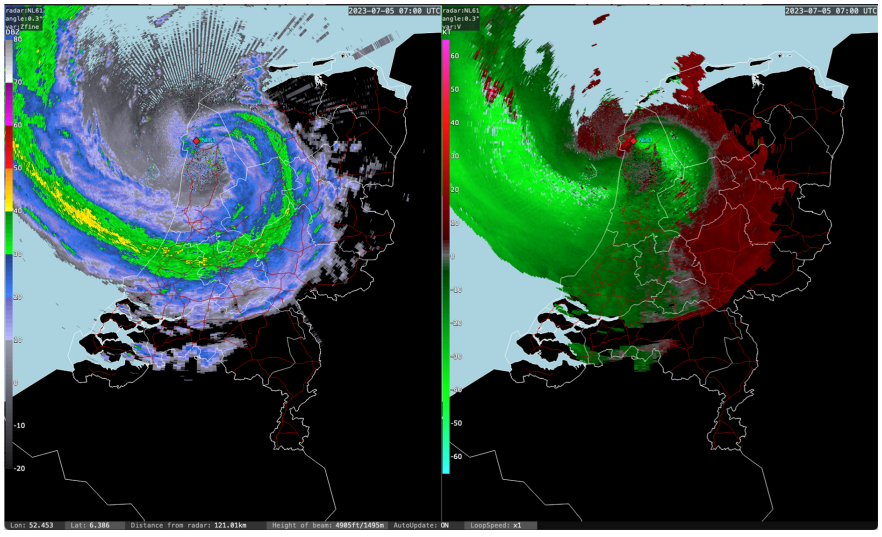

(b)

Figure 3: Radar images from the radar tower in Den Helder. left Image: reflectivity (dBZ), right image: radial velocity (KT) . Top image (a): 0300 UTC, bottom image (b): 0700 UTC.

Between 0300 UTC and 0700 UTC (Fig.3b), Storm Poly rapidly becomes more organized. By 0700 UTC, the precipitation is clearly organized into a spiral structure, indicative of a mature cyclonic system. A very sharp rainband is visible, and the tightly packed green and red areas around the cyclone center indicate very strong rotational winds, particularly over IJmuiden, where there was suspicion of a SJ. Additionally, the high intensities in the frontal precipitation, combined with the sharp boundary in the wind field corresponding to the inner edge of the frontal precipitation, stand out, suggesting a partly convective nature.

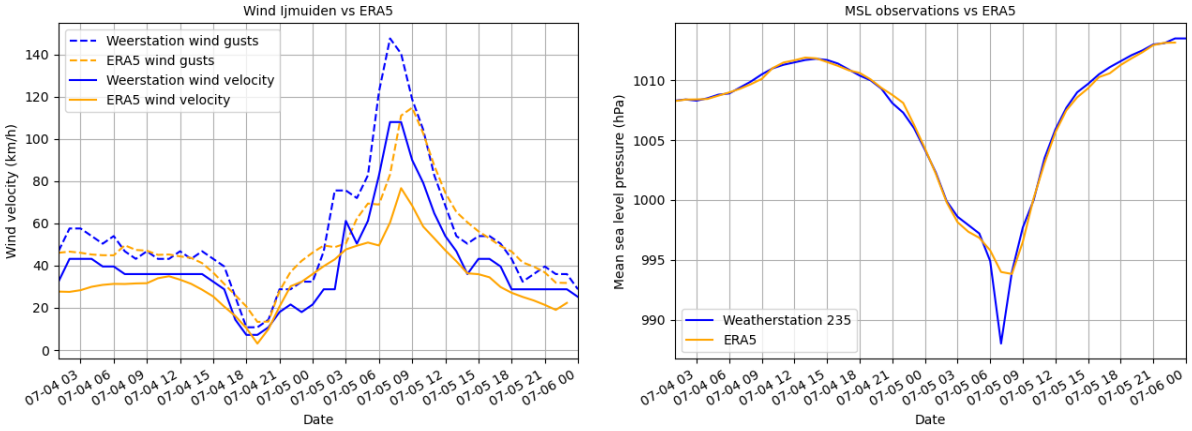

(a) (b)

Figure 4: Comparison of the weather station observations (blue) and ERA5 dataset (orange) of wind velocity and max hourly windgusts at IJmuiden (a) and MSLP at De Kooy (Den Helder) (b).

Comparing ERA5 reanalysis wind data versus observed wind speeds reveals the recorded maximum wind gust of 146 km/h at the IJmuiden station alongside the hourly average wind speed (Fig.4a). It can be observed that the ERA5 reanalysis tends to greatly underestimate the peak wind gusts and average wind speed, although it accurately captures conditions outside the storm's duration. Similarly, Fig.4b presents the minimum MSLP, where ERA5's accuracy diminishes primarily with the extreme values at the center of Storm Poly, suggesting that while ERA5 effectively models general atmospheric conditions, its precision diminishes when encountering the storm's most intense aspects. The ERA5 reanalysis data also reveals difficulties in accurately pinpointing the timing of Storm Poly's peak winds, with its maximum values occurring an hour later than those observed. This is attributed to the coarse resolution of ERA5 combined with the relatively small size of Storm Poly.

The CY46 dataset illuminates a complex interaction in Storm Poly, revealing, as suggested by the radar imagery in Fig.3, not one but three distinct systems at the lower levels (what's in a name). As depicted in Fig.5, these systems are observable in the 950 hPa wind field at 0500 UTC, eventually merging into a single, larger system that occurs during Poly's rapid intensification. This phenomenon is potentially indicative of a watered down version of the Fujiwhara effect (Fujiwhara, 1921) which describes the interaction between two cyclones in close proximity of each other and can significantly impact the development, trajectory, and strength of cyclones. This partly explains the model's disagreement in Fig.6 about the trajectory of Storm Poly and the extreme development of Storm Poly that occurred west of the Netherlands in a data-sparse region. The intensity of the low-pressure center only became fully visible when it crossed the coastline. Additionally, the timescale on which it occurred was exceptionally short.

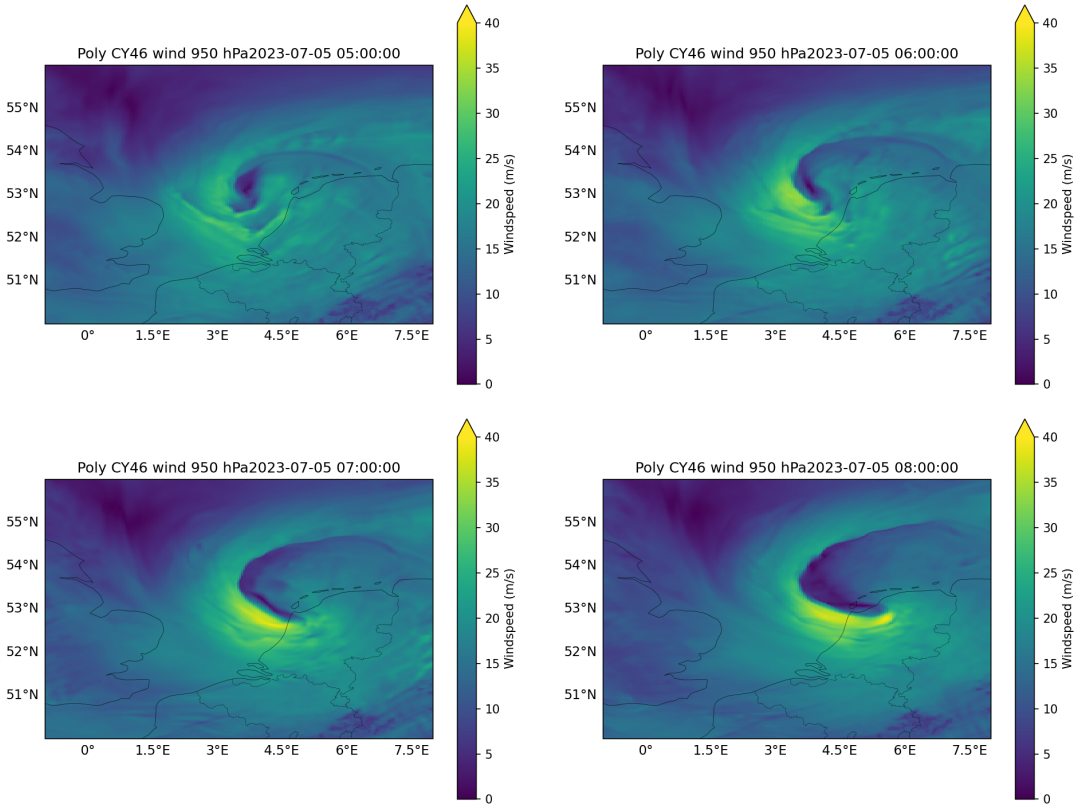

Figure 5: Windspeed at 950 hPa at (from left to right) Top: 0500 UTC, 0600 UTC, Bottom: 0700 UTC and 0800 UTC.

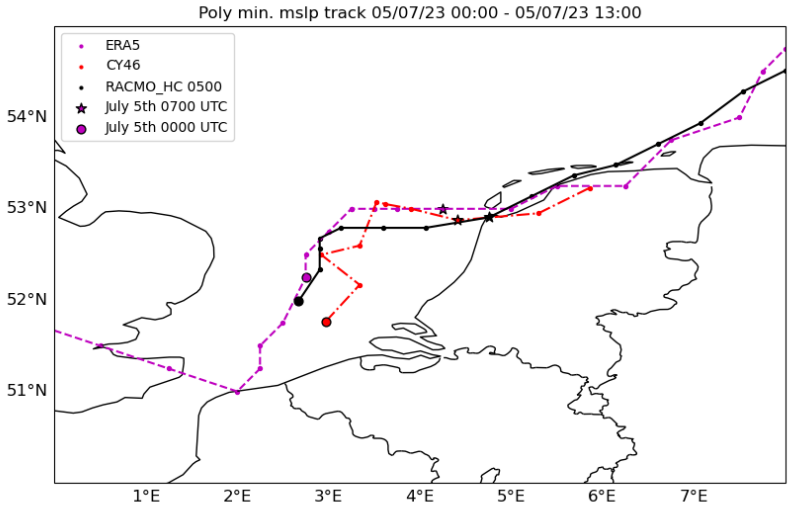

Figure 6: Track of Storm Poly as per minimum MSLP in the CY46 (red dot-dashed), ERA5 (purple dashed) and RACMO's latest HC run (black line). The star highlights the moment of assumed landfall at 0700 UTC.

3.2 Exploring the Sting-Jet Hypothesis

Utilizing the ERA5 Reanalysis dataset, we conduct an extraction of streamlines within the vicinity of the presumed SJ activity. We employ this initially on Storm Ciarán (1700 UTC 01-11-23) as a case study where SJ signatures were evident in both satellite and radar data. This enhances our understanding of SJ characteristics in the reanalysis framework.

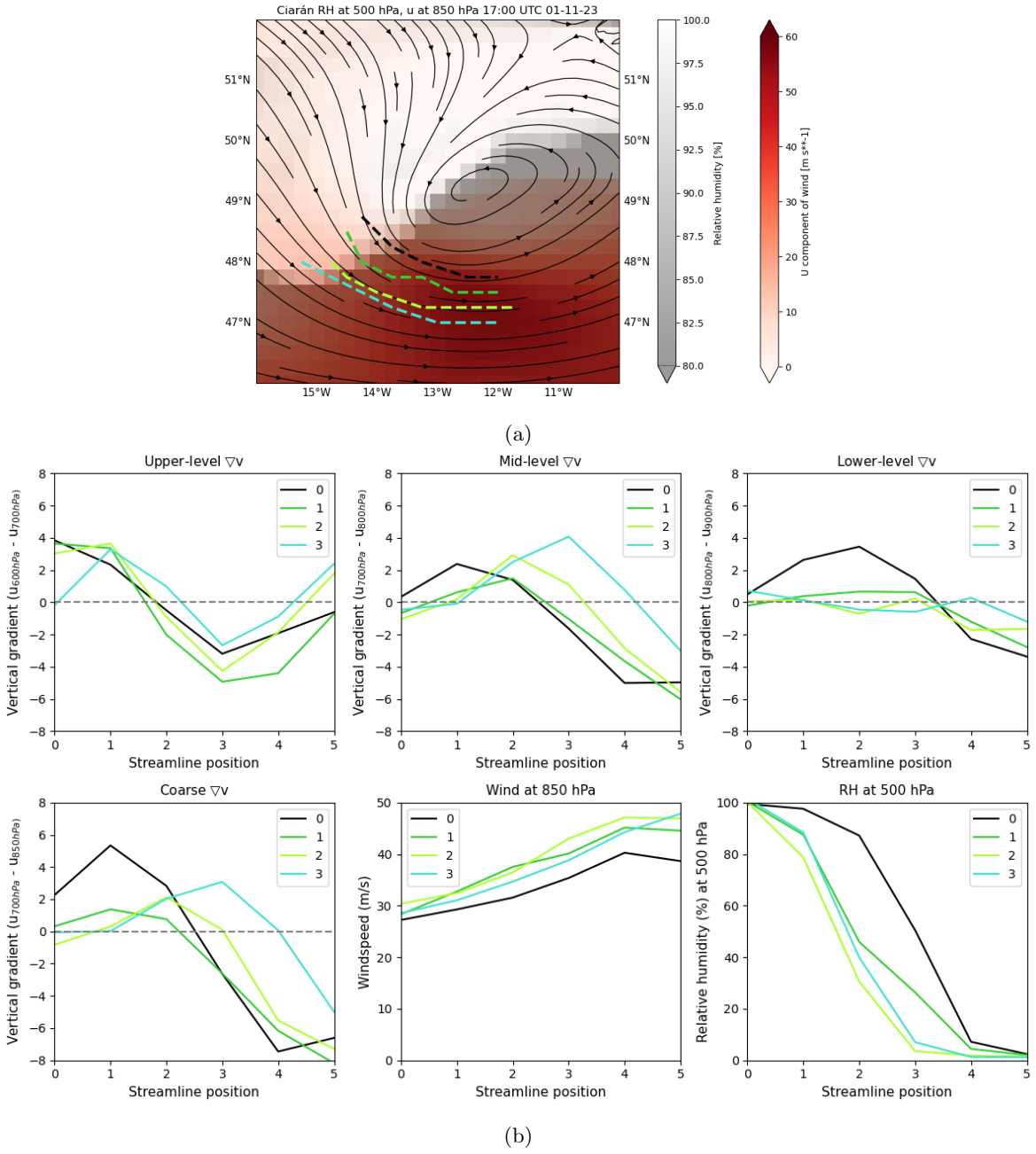

(a)

(b)

Figure 7: ERA5 Windstorm Ciarán 01-11-23 1700 UTC extracted streamlines (a) and vertical zonal wind gradient from left to right upper row: 600-700 hPa, 700-800 hPa and 800-900 hPa, bottom row: vertical zonal wind gradient 700-850 hPa, wind velocity at 850 hPa and RH at 500 hPA along the streamlines from west to east.

The results illustrated in Fig.7 confirm the presence of SJs in Storm Ciarán, evidenced by a discernible reversal of the vertical wind gradient at the upper and mid-levels, diverging from the cloud head and away from the bent-back occlusion. This reversal, indicative of slantwise descent, coincides with a notable increase in wind velocity at 850 hPa of at least 10 m/s and a significant decrease in RH, nearing a 100% reduction along the streamlines. These observations collectively confirm the occurrence of multiple SJs within Storm Ciarán on the 1st of November at 1700 UTC.

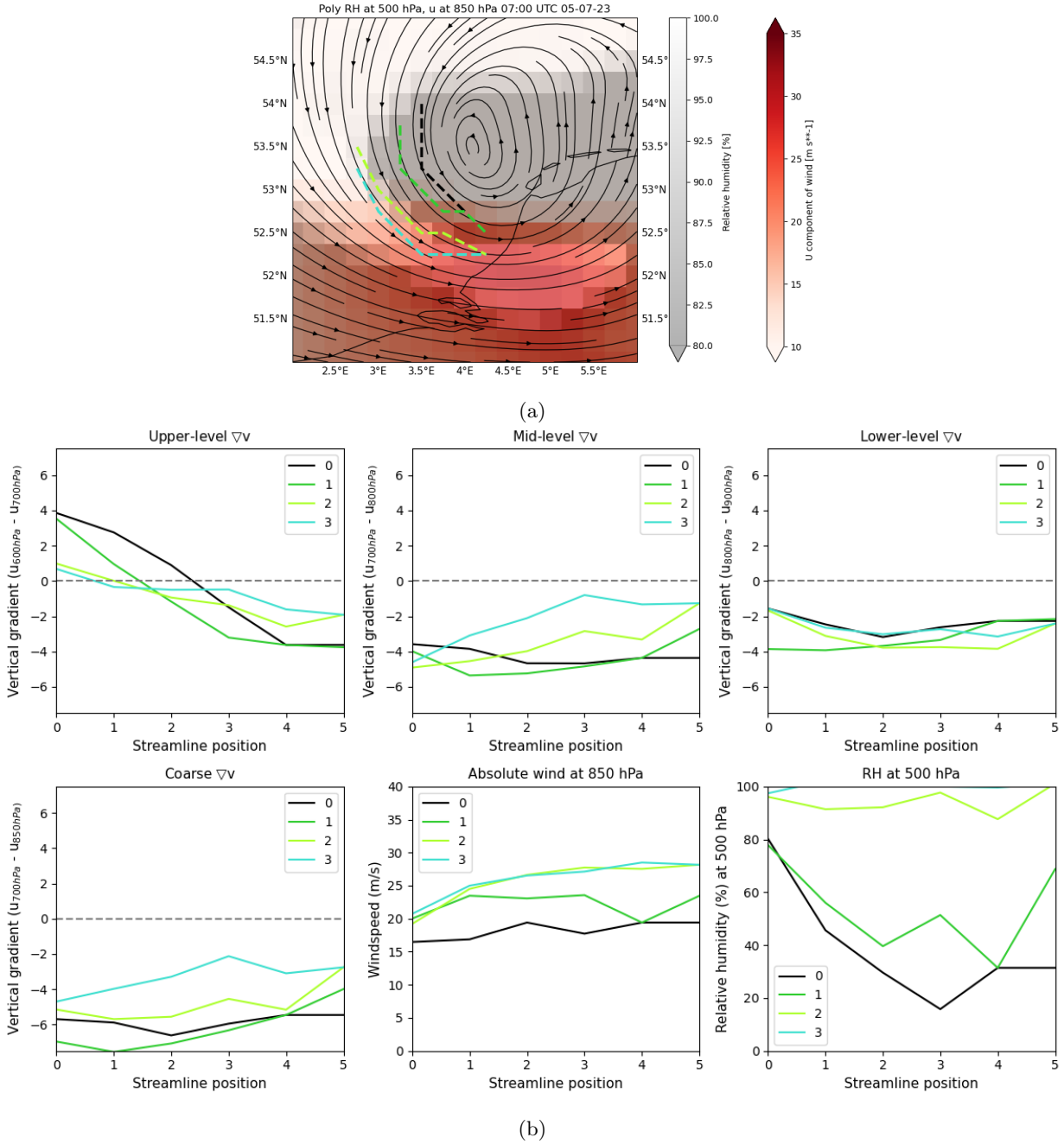

Figure 8: ERA5 Storm Poly 05-07-23 0700 UTC extracted streamlines (a) and vertical zonal wind gradient from left to right upper row: 600-700 hPa, 700-800 hPa and 800-900 hPa, bottom row: vertical zonal wind gradient 700-850 hPa, wind velocity at 850 hPa and RH at 500 hPA along the streamlines from north-west to east.

When comparing these observations with those for Storm Poly in the ERA5 dataset, as depicted in Fig.8, no SJ phenomena are evident along the selected streamlines. Although a shift from a positive to a negative vertical gradient is noted at upper levels, this pattern does not extend to mid and lower levels, where the gradient remains negative throughout the track. This pattern indicates stronger zonal winds at lower atmospheric levels compared to upper levels, negating the presence of slantwise descent. Additionally, the data does not demonstrate a significant increase in wind velocity at 850 hPa, nor does it fulfill the criteria for the required drop in RH along these streamlines, suggesting the absence of SJ conditions in Storm Poly.

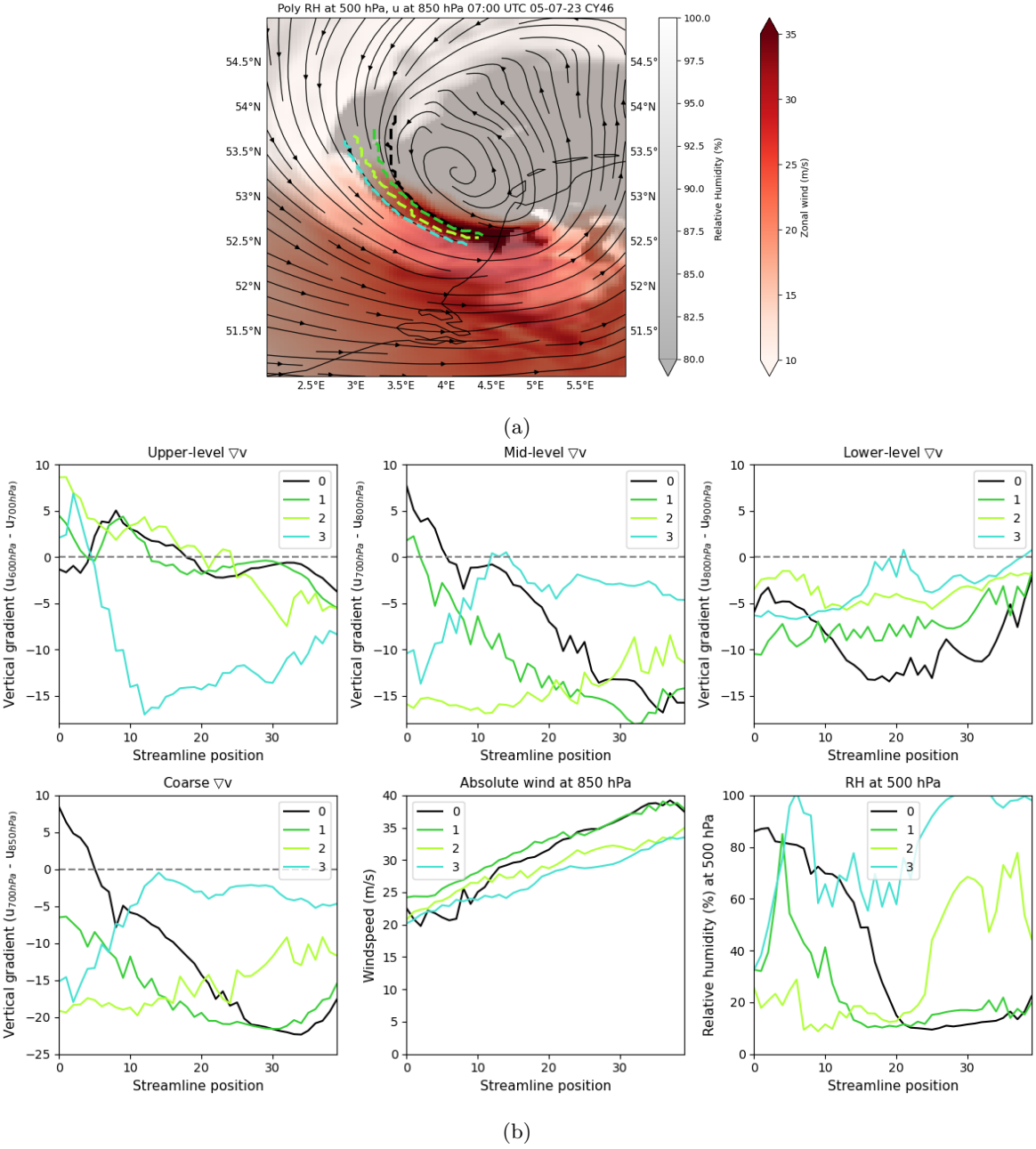

Figure 9: Storm Poly 05-07-23 0700 UTC extracted streamlines in CY46(a) and vertical zonal wind gradient from left to right upper row: 600-700 hPa, 700-800 hPa and 800-900 hPa, bottom row: vertical zonal wind gradient 700-850 hPa, wind velocity at 850 hPa and RH at 500 hPA along the streamlines from north-west to east.

Applying the same analysis to the CY46 dataset reveals a more complex scenario as illustrated in Fig.9. Streamlines 1 through 3 show an amplified version of the vertical gradient pattern observed in Fig.8. Notably, wind velocity at 850 hPa increases by over 10 m/s across all streamlines, though RH exhibits erratic behavior for streamlines 1-3. Specifically, the innermost streamline (represented by a black line) suggests a SJ-like process not detected in the ERA5 analysis, likely due to ERA5's coarser resolution and the scale differences between Storms Poly and Ciarán. This analysis indicates a mid-level reversal from positive to negative vertical gradient, particularly between 700 and 850 hPa, marked by the sharpest wind velocity increase at 850 hPa ($\rangle$15m/s) and meeting the required decline in RH at 500 hPa.

These results suggest that there might have been some sort of SJ present. However, it is most likely that the SJ was not the primary cause of the strongest winds observed. This conclusion is drawn from the observation that the highest wind speeds were consistently at the surface along the entire streamline, rather than originating from mid-levels towards the surface. Therefore, while the SJ-like feature was present, the strongest winds can be attributed to low-level processes along the streamline rather than the SJ itself.

Identifying a SJ in a storm with Poly's size presents significant challenges. In this analysis, streamlines are manually selected using a streamplot in Python. The ability to identify a SJ was dependent upon the initial starting location that we picked. This method does not account for vertical wind shear, as the streamline is selected at the 850 hPa level and observations are made vertically from that point. Consequently, a curved sting jet induced by vertical wind shear may not be detected but we deem this unlikely in Poly's case as there is no strong vertical wind shear in this area. Furthermore, the area with these high wind speeds was at most a few kilometers wide. This narrow region might be difficult to detect even with the higher resolution provided by the CY46 model, especially if there is any distortion or tilting of the wind.

3.3 Poly's Vertical Structure: PV, ω and u

Since the SJ hypothesis is dismissed, we aim to determine the underlying cause of the strong surface winds observed. To explore this, we generate cross-sections through Poly's point of minimum MSLP from north to south in both ERA5 and CY46 datasets focused on potential vorticity (PV), zonal wind, equivalent potential temperature, vertical velocity, and RH. The figures presented below were created for 0700 UTC, with similar analyses conducted at hourly intervals to further investigate the storm's evolution.

Fig.10 demonstrates the low-level wind maximum formation in both datasets, with similar overall structures observed. Notably, CY46 depicts a stronger, more narrowly focused wind maximum slightly northward compared to ERA5, aligning with the timing of maximum wind speeds recorded at the IJmuiden weather station. CY46 also provides more detail due to the higher resolution of the model. Fig.10 illustrates significant upper-level PV, alongside a distinct region of high PV at lower levels. This confirms that Storm Poly likely resulted from the interaction between an upper-level system and a low-level disturbance. Over time, these two systems align, with their alignment coinciding with the period of rapid intensification of Poly. The low-level jet is situated precisely to the south of the low-level positive PV anomaly.

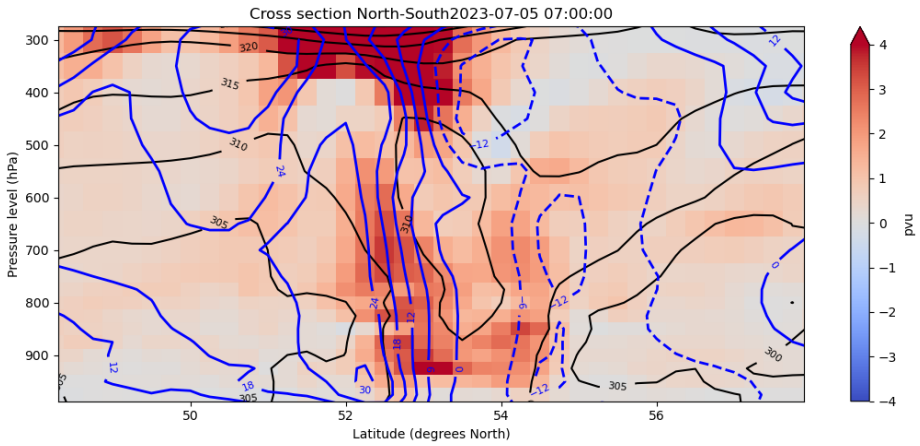

(a)

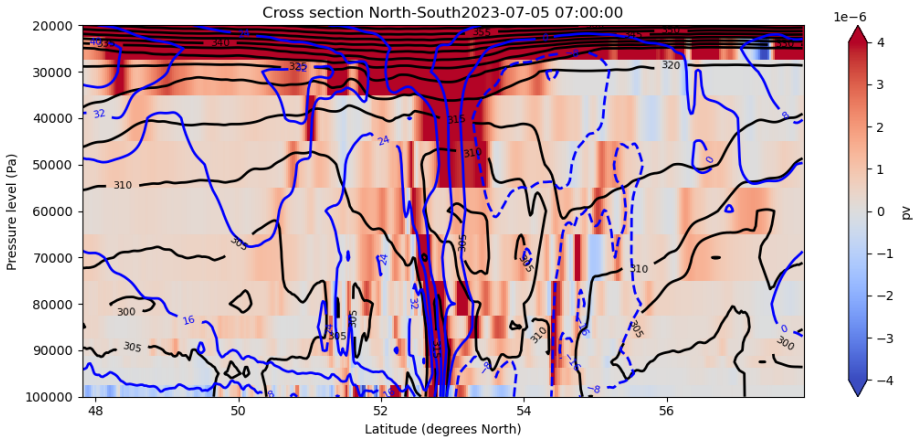

(b)

Figure 10: Cross-sections of Storm Poly on 05-07-2023 at 0700 UTC from North to South, using ERA5 (a) and CY46 (b) datasets. Blue lines depict zonal wind contours, black lines represent contours of equivalent potential temperature and the gradient colors denote units of potential vorticity.

When comparing the analysis of Storm Poly's vertical velocities within its core (Fig.11), it is revealed that ERA5 unsurprisingly inadequately captures the vertical atmospheric movements. While ERA5 indicates some upward motion north and south of the core, it fails to show distinct convection zones, unlike the CY46 dataset. Intriguingly, CY46 imagery (Fig.11b) illustrates intense upward motion on the southern side of the storm's core, closely associated with high RH. This region lies just north of the identified southern wind maxima and areas of strongest wind gusts, suggesting convection's critical influence on the storm's devastating winds, rather than a top-down approach as seen with SJs. This suggests a strong relationship with latent heating and implies the presence of warm-core dynamics, potentially indicating a subtropical mechanism at work within Storm Poly.

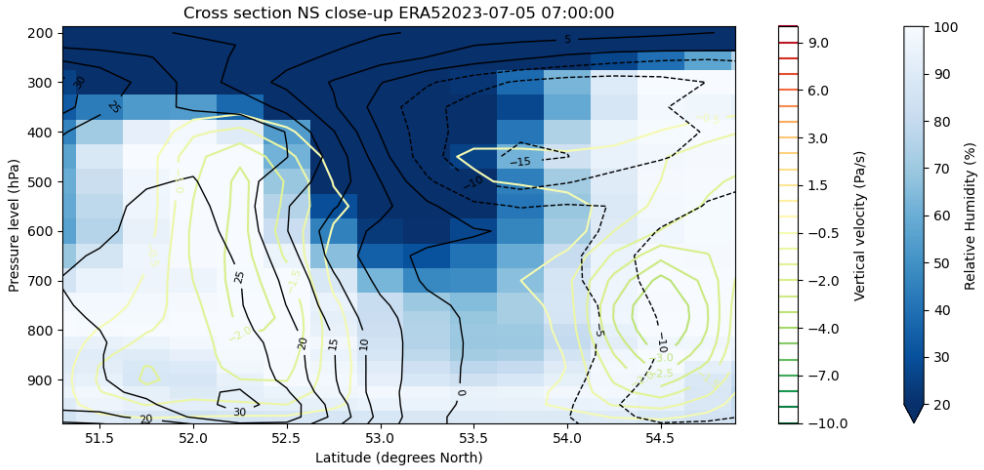

(a)

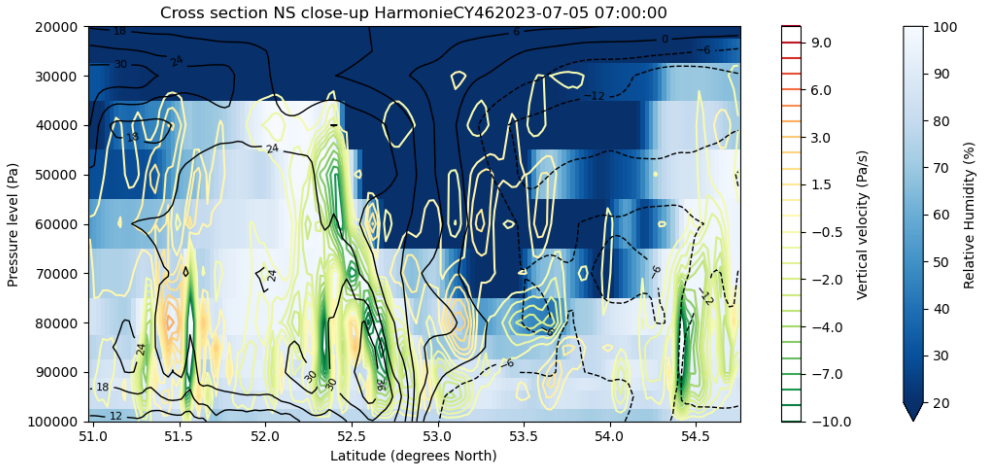

(b)

Figure 11: Cross-sections of Storm Poly on 05-07-2023 at 0700 UTC from North to South, using ERA5 (a) and CY46 (b) datasets. Black lines depict zonal wind contours, the green/red gradient contours represent the vertical velocity in Pa/s where green represents upward motion and the orange/red colours represent downward motion and the blue/white gradient colors denote the RH.

3.4 Implications of RACMO PGW Runs and Initial Conditions

Several key observations are made from the PGW simulations in RACMO (Fig.12). The control run analysis for 5 July (Fig.12b) closely mirrors the original track observed in CY46 and ERA5. However, the PGW simulation tracks show little deviation from the original track and MSLP development. This is attributed to the lack of spin-up time; Storm Poly is already present in the English Channel when the runs are initiated, so the climate perturbations do not significantly affect its development. The notable exception is the +3°C dry run, which deviates more to the east over land and consequently exhibits a higher minimum MSLP.

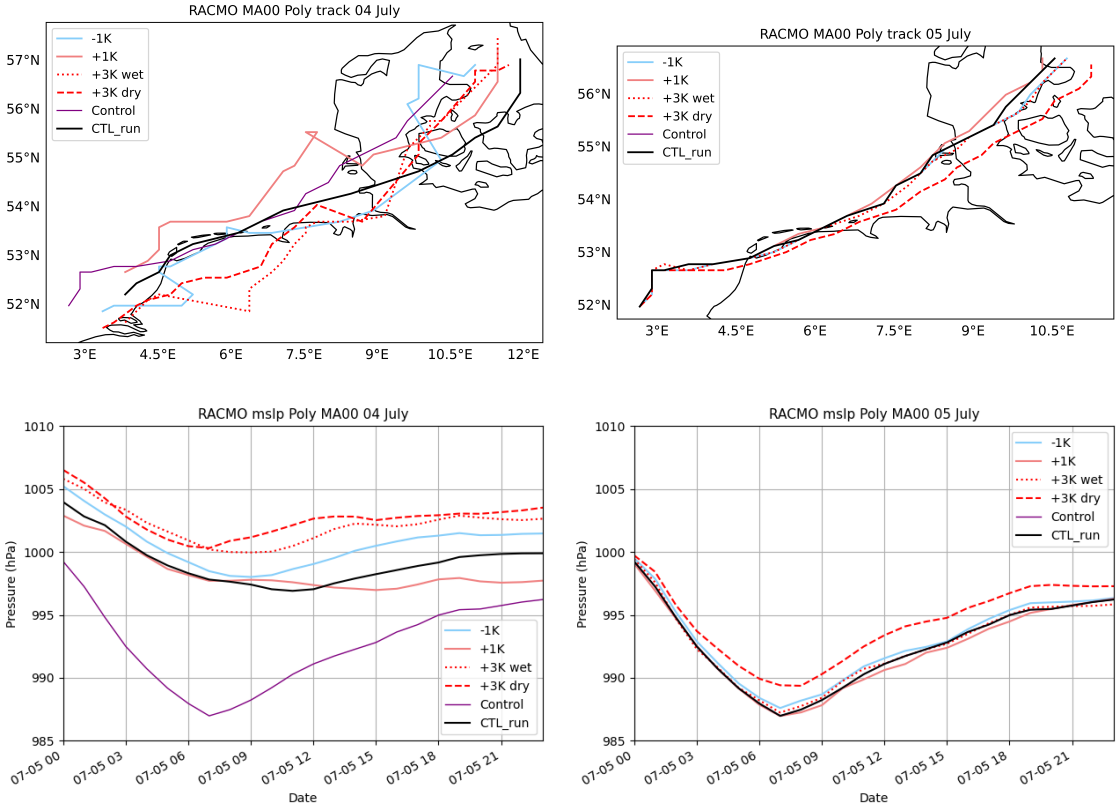

Figure 12: Storm track and MSLP of Storm Poly in RACMO's PGW simulations. Left: Simulation initiated on 4 July at 0000 UTC, using the forecast analysis. Right: Simulation initiated on 5 July at 0000 UTC, using the forecast analysis. Top panels: Storm track of Poly, determined by minimum MSLP, from 5 July at 0000 UTC to 5 July at 2300 UTC. Bottom panels: Minimum MSLP of Poly during the same period

When the simulation starts 24 hours earlier (Fig.12a), we observe the results with more spin-up time. However, the control run does not accurately reflect Poly's actual development and fails to represent the real event, indicating that the initial conditions pose a significant problem. While the tracks in the PGW simulations show more deviation from each other, any differences in storm intensity can be explained by the relocation of the track. Specifically, the +3°C dry and wet simulations are located further east and therefore have a higher minimum MSLP. This pattern is consistent across all RACMO PGW simulations: the further the forecast period precedes the 5th of July 0000 UTC, the less accurate the track becomes, and Poly is not well forecasted. Consequently, the tracks are significantly off, preventing any conclusive findings, except that a track over land results in a weaker storm, while a track over the North Sea leads to a stronger storm.The figures for the 24-hour, 48-hour, and 72-hour forecasts can be found in the appendix.

In conclusion, the model's initial conditions are crucial for accurately forecasting Poly's development. The

event is not well forecasted 24 hours before its occurrence. Therefore, for more effective spin-up time, it is important to examine the forecasts between 4 July at 0000 UTC and 5 July at 0000 UTC, as this period appears to be critical for Poly's development and prediction. The spin-up time for the PGW runs is essential to capture any effect of the changes made at the boundary of the model. With too little spin-up time, the storm will not be affected by the PGW. The combination of the needed spin-up time to obtain useful results from the PGW runs and the importance of the initial conditions to accurately capture the storm's development creates a tricky situation. While these simulations are aimed to project Poly's behavior under different climate scenarios, the results are inconclusive due to the poor representation of Poly's initial development. This complexity makes Poly a particularly difficult storm to analyze in climate simulations.

RACMO HindCast analysis

Because the forecast of Poly proved to be a difficult endeavor, as discussed in section 3.4, we examine the RACMO HC runs at 6-hour intervals starting from 3 July at 0000 UTC. Fig.13 illustrates the tracks and minimum MSLP development of Poly in these runs. Both panels show that Poly's HCs on 3 July were mostly in agreement with each other, with its track predicted further east and without significant deepening in MSLP on 5 July. This aligns with the initial prediction from KNMI's weather forecast (T. Zwagers, personal communication, 2 October, 2023).

A substantial shift is observed on 4 July, with Poly's track moving westward and the 0000 UTC run on 4 July beginning to show more deepening compared to the previous run. The 0600 UTC run on 4 July indicates an even stronger westward shift and more pronounced deepening. However, the most significant change is evident when comparing the 0600 UTC run (0406) with the 1200 UTC run (0412). From 1200 UTC on 4 July, the track closely resembles the actual event, with rapid deepening and a path that moves through the Canal and stalls over the North Sea.

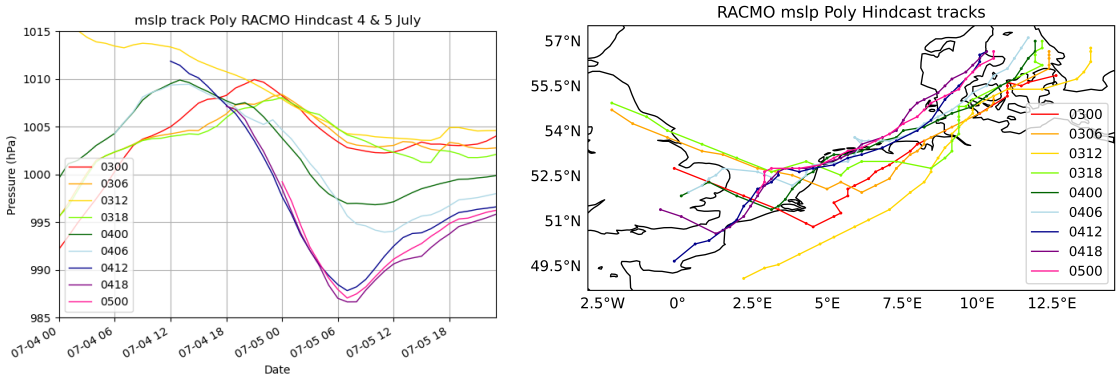

(a) (b)

Figure 13: MSLP (a) and storm track (b) of Storm Poly in RACMO's HindCast from 4 July, 0000 UTC to 5 July, 2300 UTC. Runs initiated from 3 July, 0000 UTC (0300) to July 5, 0000 UTC (0500) at 6-hour intervals.

Closer examination of the runs starting from 0600 UTC and comparing them with observations reveals that, in terms of wind velocity at IJmuiden and MSLP at De Kooy (Fig.14a and b, respectively), the forecasted values of run 0406 fall significantly short. This run barely reaches half the observed wind velocity, only peaking at 15 m/s. The other runs perform similarly to ERA5 and CY46. Interestingly, the MSLP pattern at De Kooy in Fig.14b does not perform poorly until 0500 UTC on 5 July. Up until that point, the different model runs deviate by only about 2 hPa (997 hPa vs. 999 hPa at 0500 UTC). However, from 0600 UTC to 0700 UTC, a substantial gap appears. While the 0600 UTC run's MSLP starts to rise again, the 1200 UTC

(and later) runs drop by a staggering 9 hPa (from 996 hPa to 987 hPa), reaching the lowest MSLP of 987 hPa at 0700 UTC before rising again. This suggests a very strong and relatively small low-pressure system.

Previous analysis of radar imagery and CY46 data indicated the presence of two lows within Poly, raising the possibility that the differences between these runs and the initial conditions are related to this low-level disturbance, which is difficult for models to capture far in advance. It appears that run 0406 captures the large upper-scale dynamics of Storm Poly, resulting in a track that overlaps with the observed storm-track, but fails to capture the low-level disturbance which proved to be crucial in Poly's development and intensity.

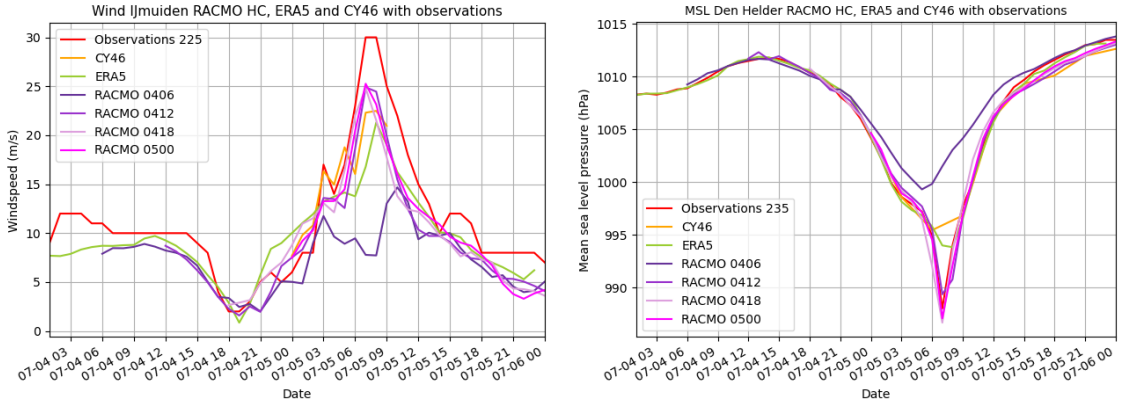

(a) (b)

Figure 14: Hourly average wind speed at IJmuiden (a) and MSLP at weather station De Kooy (Den Helder) (b) from observations, CY46, ERA5, and RACMO's HindCast runs 0406, 0412, 0418, and 0500.

To confirm this, we examine the MSLP field for both runs and the location of the jet stream, as shown in Fig.15. At first glance, there appears to be minimal difference between the runs. However, back-tracking Poly reveals that its location in run 0412 differs significantly from the run 0406. In Fig.15a, Poly is situated over Brittany for run 0412, where the MSLP is slightly overestimated in the 0600 UTC run, coinciding with the presence of convective showers at that time. In run 0406 Poly is situated over Great-Britain, where the upper-level development of Poly is present. Comparing the differences four hours later (Fig.15b), the discrepancy increases, highlighting three distinct regions where MSLP is overestimated in run 0406 and where the convective showers were eventually observed. Run 0412 places Poly precisely in this location. This suggests that the prediction of the low-level disturbance, specifically the convective showers over Brittany on the 4th of July, was crucial for Poly's rapid development and high intensity.

The development of Storm Poly is notably complex. Analysis of the RACMO HC indicates that Poly was well represented from 1200 UTC on 4 July. However, the weather office primarily relies on ECMWF forecast members, where this information was not as straightforward. Discussions with meteorologists revealed that the eventual impact of Poly on the Netherlands represented the most extreme scenario presented by the models. It appears that the upper-level system was fairly well predicted, and cause for issuing code yellow, but the presence and unpredictable convective nature of the showers over France caused the greatest uncertainty. Their interaction also affected the upper-level dynamics, ultimately resulting in a significantly different storm. The development of these showers is inherently uncertain, complicating the interaction between the two systems. Additionally, prediction is hindered by observational limitations. The showers over France only became apparent at 1200 UTC on the 4th of July; prior to this, they were still developing over the Bay of Biscay. This had a significant impact on the forecast.

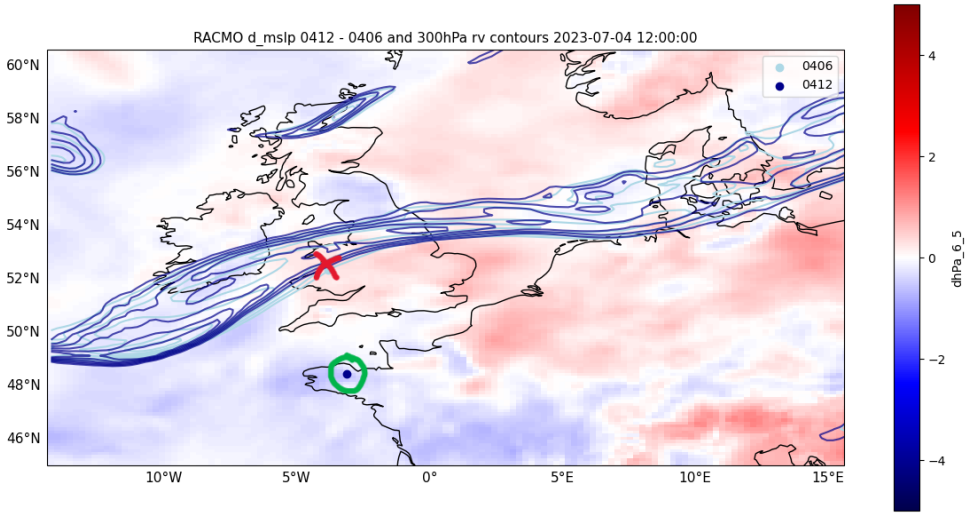

(a)

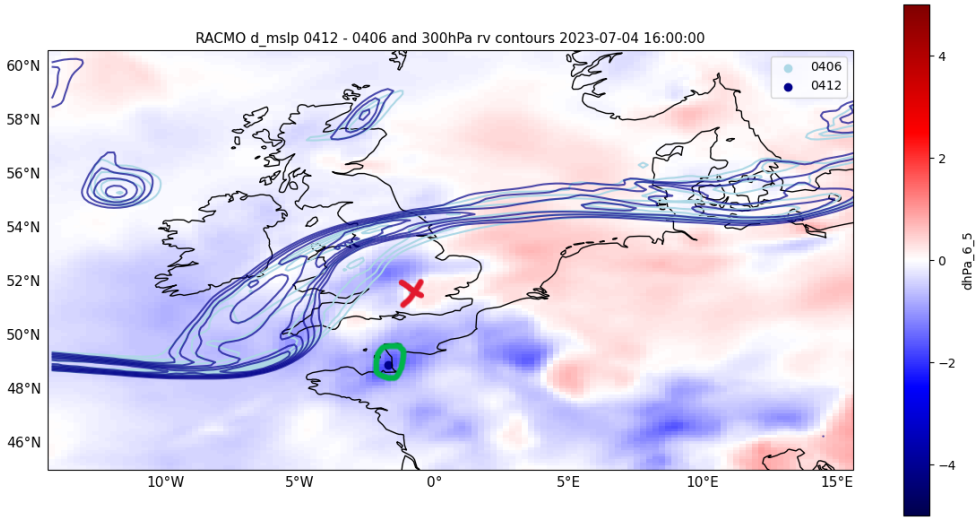

(b)

Figure 15: Map of MSLP differences and the upper-level jet between the 0406 and 0412 RACMO HindCast runs. Blue/red gradient colours show MSLP differences (0412 - 0406) initiated on 4 July at 0600 UTC and 1200 UTC. Red indicates underestimation, and blue indicates overestimation in the 0406 run, highlighting intensified showers over Brittany. The red cross marks Poly's minimum MSLP location at 0600 UTC, and the green circle marks it at 1200 UTC. Dark/light blue isolines show relative vorticity at 350 hPa, indicating the jet stream's location

3.5 The North Sea Connection: RACMO dSST

Due to inconclusive results from the PGW simulations, we designed an experiment to isolate the effects of latent heating and North Sea temperatures. We hypothesize that Storm Poly's development might be driven not by the overall heat of the climate system, but by the temperature contrast between SST and the temperature at 500 hPa, a known driver for medicanes, polar lows and subtropical cyclones over the Atlantic Ocean (Berg, 2021; Varlas et al., 2023). The PGW simulation setup reduces this temperature contrast, potentially misrepresenting Poly's connection with the North Sea. Previous research indicates that SST significantly influences the intensity of medicanes, particularly in terms of MSLP development, total precipitation, and precipitation intensity (Bui & Spengler, 2021; Varlas et al., 2023). This is attributed to increased energy fluxes enhancing deep convection within the cyclone's warm-core. Thus, we conduct RACMO simulations with altered SST scenarios ranging from -4°C to +4°C in 1°C increments (RACMO dSST).

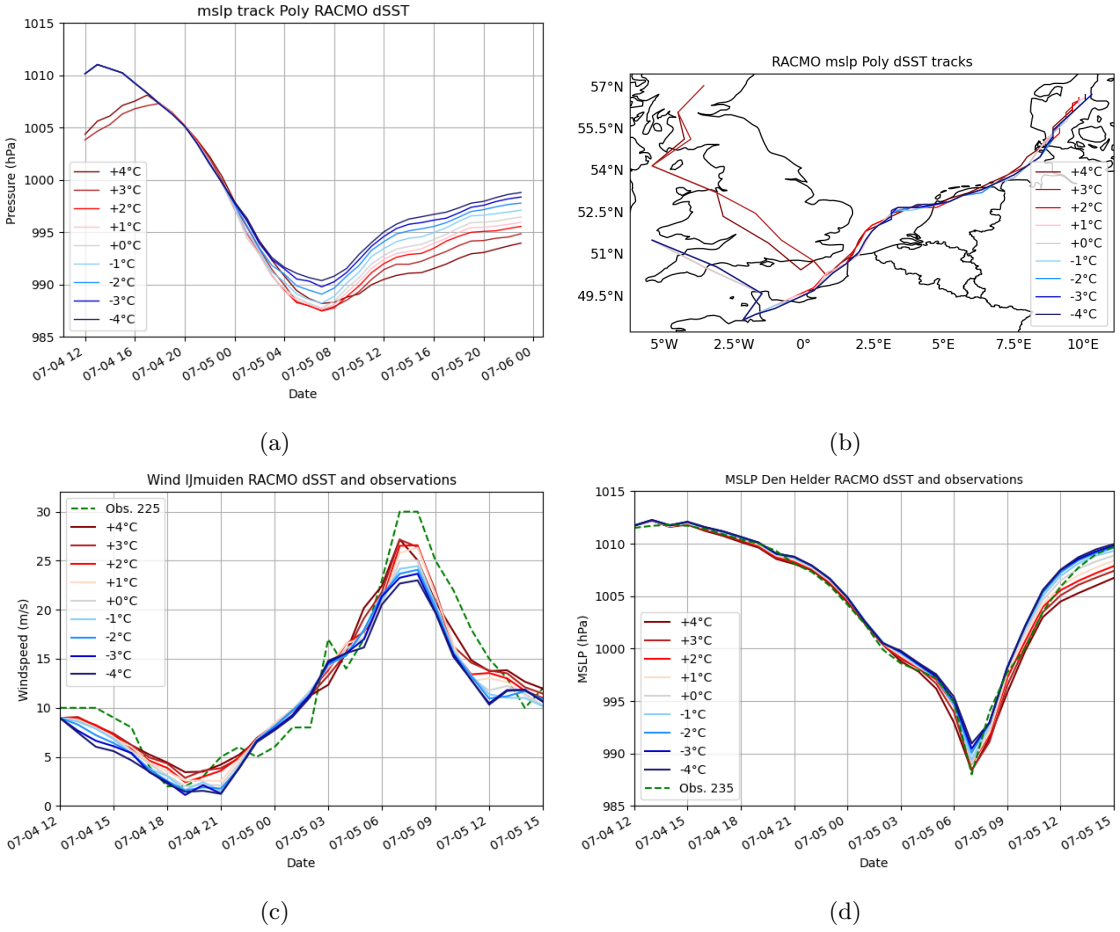

Figure 16: MSLP (a) and storm track (b) of Storm Poly in RACMO's dSST simulation from 4 July, 1200 UTC to 5 July, 2300 UTC. And comparison of RACMO's dSST simulations with observations (hatched green line) of hourly average wind speed at IJmuiden (c) and MSLP at weather station De Kooy (Den Helder) (d).

We observe a higher minimum MSLP in Storm Poly at lower SSTs in Fig.16a. Notably, rapid intensification of 2 hPa/hr is consistent across all scenarios until 5 July, 0000 UTC, reaching around 997 hPa. Beyond this point, intensification slows for lower SST runs but continues steadily for higher SST runs. Rapid intensification concludes earlier, around 0300 UTC for the -4°C run, compared to 0600 UTC for the control and +4°C runs, where Poly's minimum MSLP peaks at 991 hPa for the -4°C run and 988 hPa for the -1°C run.

Another observation is that the absolute minimum MSLP does not increase for higher SST runs compared to the control run, reaching around 987.5 hPa at 0700 UTC. The +4°C run does not drop below 988 hPa. This could be due to two factors: 1) landfall preventing further intensification, confirming warm-core dynamics, or 2) a SJ-like feature introducing cold upper-air into the storm's core, disrupting latent heating. We consider the former more likely.

The storm tracks (Fig.16b) are almost identical, ruling out track deviations over land or sea as explanation for MSLP differences. Fig.16c illustrates that varying SST scenarios also result in correspondingly higher or lower wind speeds, which is in line with results from previous research on the influence of SSTs on cyclone development (Bui & Spengler, 2021; Sinclair et al., 2020).

dSST	min. MSLP	Windspeed		Cumulative precipitation (mm)		
°C	hPa	km/h	Bft	r = 50 km	r = 100 km	r = 150 km
+4	984.2	103.3	11	76.7	59.3	50.3
+3	984.3	105.1	11	76.2	60.7	50.4
+2	985.5	103.1	11	85.9	65.6	53.9
+1	986.5	102.3	10	80.5	64.0	53.3
0	987.8	101.0	10	78.7	63.2	53.3
-1	988.2	99.1	10	75.6	62.4	53.2
-2	989.1	96.9	10	73.0	61.6	52.7
-3	989.8	92.9	10	70.9	61.1	52.5
-4	990.4	90.0	10	69.2	61.6	52.6

Table 2: Results of Storm Poly in RACMO dSST simulations. The table shows the minimum MSLP of Poly, maximum hourly average 10 meter wind speed (in km/h and Beaufort scale), and cumulative precipitation (in mm) at multiple radii of 50 km, 100 km, and 150 km around the storm. The cumulative precipitation is measured from 4 July, 12 UTC until 5 July, 12 UTC and values are extracted only from grid cells with a precipitation rate over 0.0001 kg/m^{2}s.

Comparing the overall characteristics of Storm Poly in the RACMO dSST simulations (Table 2), we observe that in the higher SST runs, Poly reaches a lower minimum MSLP compared to the control, indicating a stronger storm. Higher SSTs correlate with increased overall wind velocities (up to 4 km/h stronger) and larger areas affected by strong winds (Fig.17), signifying intensified storms. Conversely, lower SSTs result in a significant decrease in wind velocity (10 km/h in the -4°C run). Additionally, ncreased SSTs generally lead to higher total precipitation, with the largest differences occurring near the storm's center (r = 50 km), showing an increase of up to an average 7 mm in that area. This pattern is evident in the regression analysis, particularly over the area where the storm's occluding front intensity is greatest (Fig.18b). Lower SSTs result in a more substantial decrease in precipitation, up to 8.5 mm.

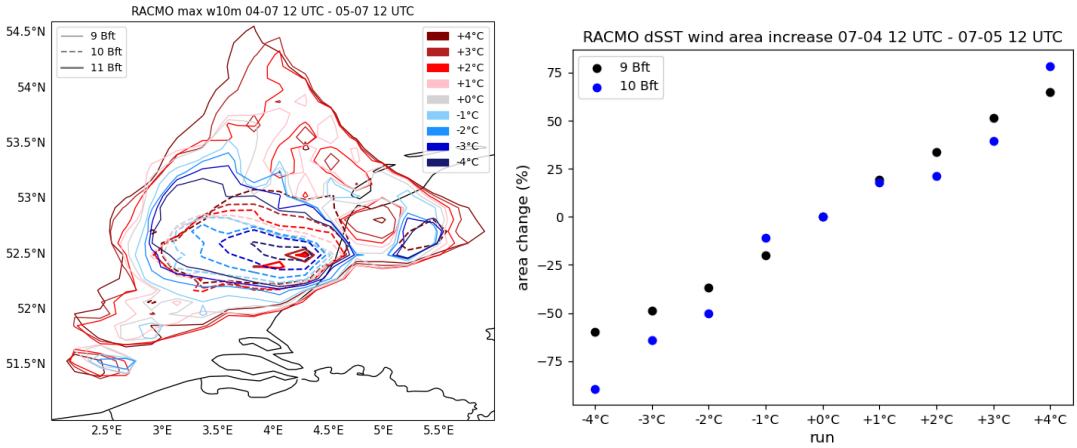

(a) (b)

Figure 17: Changes in windfield in the RACMO dSST simulation (a) Maximum 10 meter hourly average wind velocity over 24 hours (4 July 12 UTC - 5 July 12 UTC) represented by isolines of 9 Bft, 10 Bft, and 11 Bft. (b) Area change in percentage of the 9 Bft and 10 Bft area of the storm.

An interesting feature is observed in the higher SST runs: the +1°C and +2°C runs exhibit the most significant changes in precipitation. This is likely due to the storm's increasing size with higher SSTs, which expands the area within a radius around the storm where precipitation exceeds 0.0001 kg/m²s, thereby skewing the total precipitation calculation which increases exponentially in quite a large area (Appendix26). The maximum wind speed is observed in the +3°C run. Figures 17 and 18a show an increase in the storm's area of impact, with the region experiencing storm-force winds (9 Bft) growing linearly with higher SSTs compared to the control run.

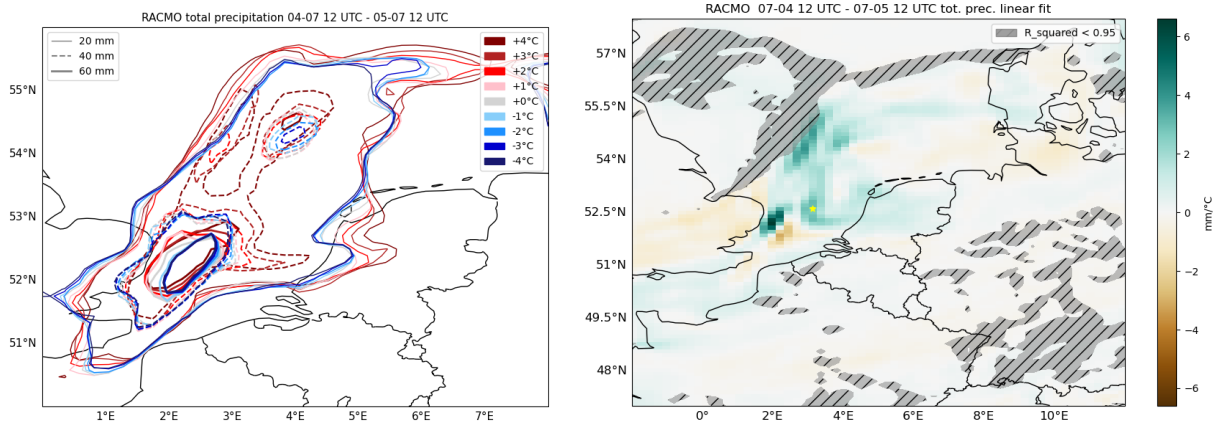

(a) (b)

Figure 18: Maps illustrating the change in cumulative precipitation in the RACMO dSST simulation (a) Total precipitation isolines of 60 mm, 40 mm, and 20 mm over 24 hours (4 July 12 UTC - 5 July 12 UTC). (b) Linear regression coefficient in precipitation, indicating an increase in total precipitation with higher SSTs. Hatched areas represent regions where the R-squared value is lower than 0.95.

The influence of the SST propagates all the way to top of the troposphere as the geopotential thickness diagram (Fig.19) reveals a reverse S-shape in the vertical profile. This pattern indicates a shallow warm-core at the surface and a cold-core in the upper levels, observed in both ERA5 data and RACMO dSST model

runs. The lower-tropospheric thickness asymmetry of Storm Poly illustrates its hybrid phase over the North Sea, characterizing it as a frontal warm-core cyclone (Evans & Hart, 2003). At 0500 UTC, when Poly is located over the North Sea, all model runs, including ERA5, depict a clear shallow warm-core. There is sharp contrast between ERA5 and RACMO visible between the upper-level and lower-level of the diagram. Where the two models seem to agree largely on the upper-level geopotential asymmetry, this is not the case for the lower-level (warm-core) intensity. This is probably the result of ERA5's struggle to resolve the (vertical) wind velocities that are integral to warm-core dynamics. Fig.11 illustrates this when comparing ERA5 to CY46.

Comparing the RACMO dSST runs we can observe that the upper-tropospheric thickness asymmetry's of the lower SST runs are slightly more slanted to the right, indicating a stronger upper-level cold-core. By 0700 UTC, the shallow warm-core becomes less pronounced in all runs, taking on a more hybrid form, with the -4°C and -3°C SST runs showing hardly any indication of a shallow warm-core. After landfall at 0900 UTC, a distinct helix-like pattern emerges between the lower and higher SST runs. In the higher SST runs, a warm-core is still present, and the upper-level cold-core is visibly less pronounced compared to the lower SST runs. The higher SST seems to enhance the warm-core dynamics and therefore promotes more deep convection which also reduces the upper-level thermal gradient. On top of that, we suggest that the enhancement of the helix-pattern over time is an artefact of the application of a uniform dSST field over water without changing any conditions over land. This reduces the large scale baroclinicity in the higher SST runs with relatively warm waters to the north of the storm and more land surface to the south and this reduces the strength of the upper-level cold-core driven by the large-scale circulation. For the lower SST runs this effect is the opposite so the upper-level trough deepens further, especially after landfall.

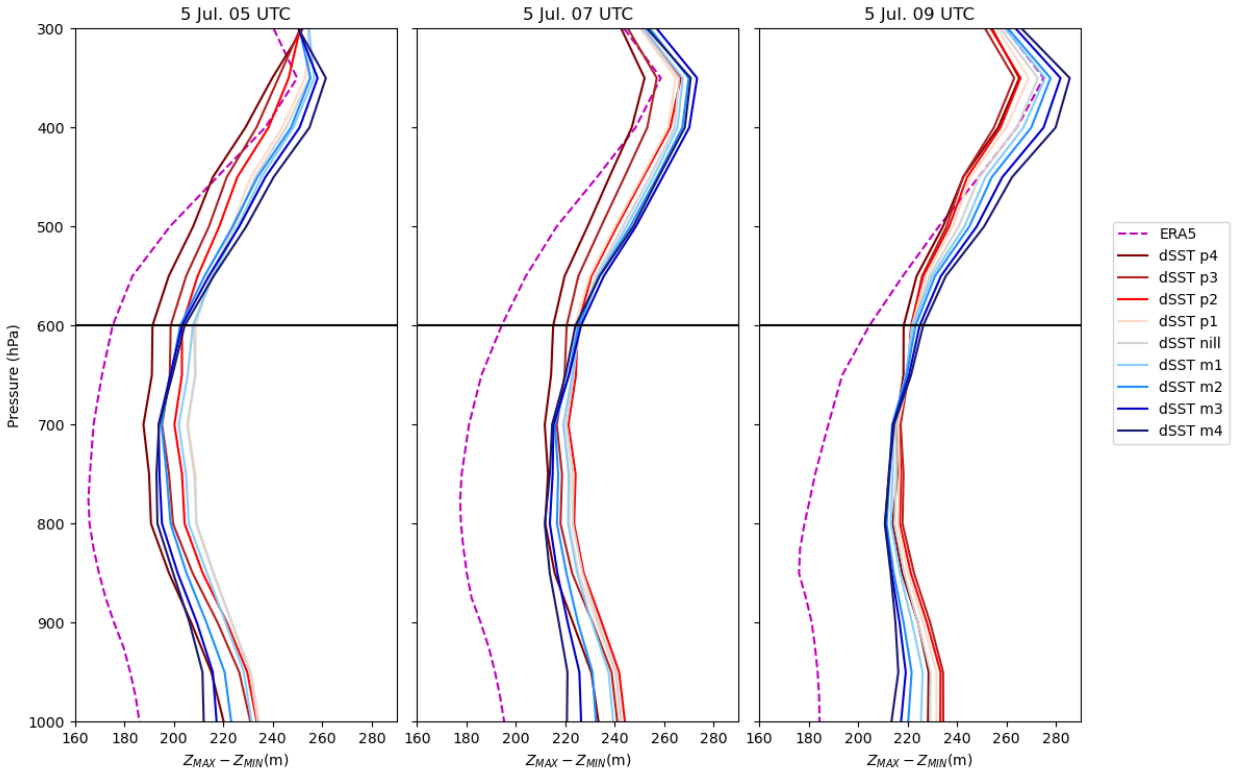

Figure 19: Hart-thickness diagram of Storm Poly depicting its shallow warm-core and hybrid evolution. The ERA5 data (purple hatched line) and RACMO dSST data (blue to red lines) show the difference between the highest and lowest geopotential heights (Z_{max}-Z_{min}) at pressure levels within a 600 km radius of the cyclone center.

There are two main effects of the SST on the vertical profile of the storm: the effect on the surface-coupling and convection, and the effect on the large scale baroclinicity affecting the large-scale dynamics. Therefore, SST plays a crucial role in the cyclone's nature, with high SST supporting warm-core or warm seclusion dynamics, and lower SST leading to a more ETC nature. However, the question of whether Storm Poly was the result of abnormally high SSTs remains partially unresolved. In the RACMO dSST simulations, we could only utilize the runs where Poly was accurately represented. These runs featured the pre-existing convective showers over Brittany. Without these showers, and their subsequent interaction with the upper-level trough, Poly did not intensify.

It is evident that the rapid development of Storm Poly, along with the associated precipitation and wind speeds, was influenced by the SST of the North Sea. Thus, we can conclude that a positive temperature anomaly over the North Sea does affect storm development. However, this does not provide definitive evidence that the SST anomalies were not the cause of Poly's bombogenesis. Due to the timing of our model runs and the weakened version of Poly in earlier simulations (before 1200 UTC), regardless of increased SSTs, we cannot yet determine the extent to which these showers were influenced by the SST of the Atlantic Ocean as these showers were not accurately represented in earlier runs. However, it is anticipated that climate change will increase the intensity and frequency of such convective showers in the future (Bui & Spengler, 2021). On top of that, these showers were mainly present over land near the west coast of France during their initial interaction with Storm Poly, further complicating their relationship with the SST.

3.6 Phase-space diagram

The left plot of the phase space diagram of Storm Poly (Fig.20) illustrates that Poly initially starts as an asymmetric cold-core cyclone on 4 July. Over time, the parameter B decreases, indicating increasing symmetry. By 0400 UTC, Poly achieves a shallow warm-core status with $-V_T^L > 0$. At 0700 UTC, the time of landfall, Poly is classified as an asymmetric shallow warm-core. After landfall $-V_T^L$ quickly reduces towards 0.

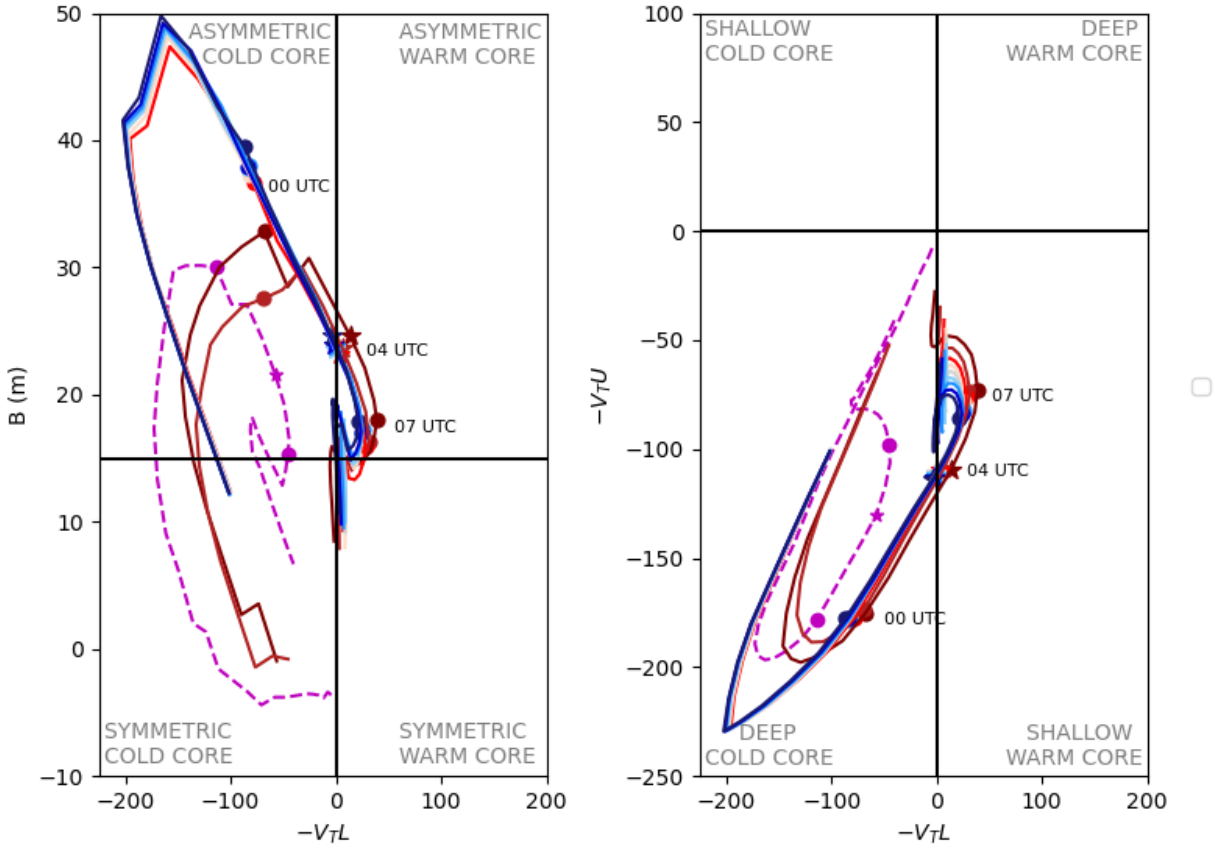

Figure 20: Phase space (Hart) diagram of Storm Poly using ERA5 data and RACMO dSST data

As discussed in the methods section, phase space diagrams are often used to distinguish between different cyclone life cycles. For example, it can be used to determine when a TC starts and finishes ET. ET starts when $B > 15$ and ends when $-V_T^L < 0$ in the North Atlantic (Studholme et al., 2015). Fig.21 illustrates this conceptually in a phase space diagram. Comparing this to Fig.20 the patterns appear very similar, although Poly undergoes the exact opposite transition and never becomes a deep symmetric warm-core. Poly also exhibited tropical characteristics, such as the strongest winds occurring close to the cyclone's center at the lower levels, distinguishing it from a typical cold-core ETC. Although identifying hybrid or SCs and their role in cyclone phase transitions remains a significant challenge (Wood et al., 2023), it appears that Storm Poly belongs in this category. With $-V_T^L > 0$ and $-V_T^U < 0$, Poly is classified as a hybrid cyclone following the criteria of Evans and Braun (2012). Despite these observations, Storm Poly cannot officially be classified as a SC according to the conditions proposed by Gozzo et al. (2014). The upper levels are too cold, with $B < 25$ m, $-V_T^L > -50$, and $-V_T^U > -10$. Moreover, Poly did not maintain this hybrid structure for more than 36 hours.

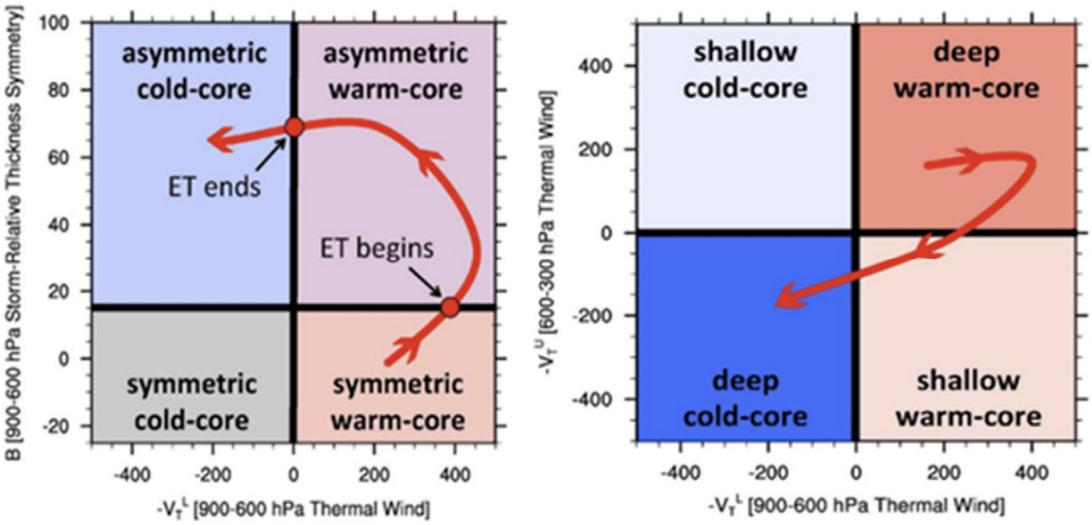

Figure 21: CPS diagrams showing the phase space evolution of ET according to (left) B and $-V_T^L$ and (right) -V_T^L and V_T^U. Adapted from Zarzycki et al. (2017). From Wood et al. (2023)

However, this behavior shows striking similarities with SC Raoni. Raoni was a subtropical storm that developed near the boundary of Uruguay and southern Brazil in June 2021 (Reboita et al., 2022). Initially exhibiting extratropical characteristics, Raoni underwent subtropical transition (ST) and was named by the Brazilian Navy at 1200 UTC on 29 June 2021. The cyclone originated from a trough from the Pacific at mid-upper levels that crossed the Andes Mountains. The transition to a SC was driven by the acquisition of a warm seclusion with strong surface heat fluxes, a deep moist troposphere, and an upper-level cut-off pattern (Reboita et al., 2022). Raoni also occurred over positive SST anomalies with the air over the sea surface slightly cooler than the SST (15 °C over an SST of 16 °C SST). Guishard et al. (2009) did note that SCs can form under seemingly unfavorable SST conditions with SSTs as low as 16 °C. The North Sea had an average SST of 15.95 °C according to ERA5 data, aligning with these observations. And according to the study by Reboita et al. (2022), a SK cyclone undergoing ST tends to remain semi-stationary due to the semi-stationarity of the surface low (warm seclusion). This occurred with both Raoni and Poly. Although the two storms differ significantly in size, with Raoni being much larger than Poly, comparing the phase-space diagrams of the two cyclones (Raoni's can be found in Appendix Fig.28) reveals striking similarities. Raoni starts as an asymmetric deep cold-core and then goes through ST, becoming a symmetric shallow warm-core. Though Poly never becomes a symmetric cyclone, it appears that Poly started ST but failed to complete it.

Another possibility is that Poly can be more accurately classified as a warm-seclusion ETC with subtropical characteristics (Fig.22). A warm seclusion storm occurs when the interaction between the cold and warm fronts results in the detachment of a portion of the cold front from the cyclone's center. This detached segment then moves eastward, intersecting the warm front at a right angle (Shapiro & Keyser, 1990). This phenomenon, referred to as a frontal T-bone fracture, is characterized by the entrapment of warm air within the cyclone's core, forming what is commonly called a bent-back warm front. This type of storm includes the most intense systems that reach Europe, featuring wind speed maxima of 22.5 ± 2.4 m/s and average pressure minima of 963 ± 14 hPa. Warm seclusion events are often associated with rapid deepening, typically around 30 hPa over two days (Dekker et al., 2018). Poly experienced a pressure drop of 14 hPa in 12 hours, but only reached a minimum pressure of 988 hPa and achieved a maximum hourly average wind speed of 30 m/s. It is possible that Poly was some sort of warm-seclusion cyclone. However, convection and the connection to the North Sea are key factors that distinguish Poly from a typical warm-seclusion storm. In warm-seclusion storms, the strongest winds are most commonly found on the southern side of the rainband. In contrast, Storm Poly's strongest winds are found inside the storm, which is more indicative of eyewall dynamics more commonly seen in (sub-)tropical cyclones.

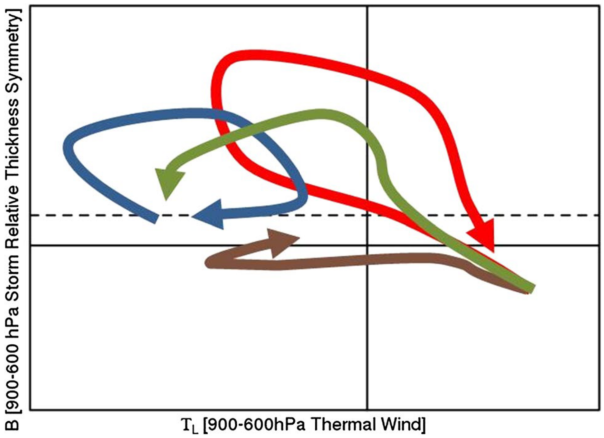

Figure 22: Schematic picture showing the different cyclone stages within the cyclone life cycles. The *blueline* represents the extratropical life cycle, *brown* the tropical life cycle, *green* the extratropical transition life cycle and *red* the warm seclusion life cycle. *Dashedline* represents the threshold value of B = 10 m. From Dekker et al. (2018)

The phase space diagrams do not provide a definitive conclusion regarding the nature of Storm Poly. Firstly, the Hart-thickness diagrams indicate that the storm features a shallow warm-core. In particular, the right panel of Fig.19 suggests that the boundary between the upper and lower levels lies at approximately 650/700 hPa, rather than 600 hPa. By adjusting the phase-space diagram parameters (low-level: 1000 hPa-700 hPa, upper-level: 700 hPa-400 hPa), ERA5 classifies Storm Poly as a shallow warm-core at 0700 UTC. This adjustment reveals increased symmetry, with B reaching nearly 15, and a more pronounced difference between higher and lower SST runs. Specifically, $-V_T^U$ is stronger in the lower SST runs, consistent with the observation that the upper level strengthens with lower SST. Additionally, Storm Poly could have been classified as a shallow warm-core earlier, with $-V_T^L$ becoming positive at 0100 UTC and approaching 100 around 0700 UTC. This revised delineation highlights the hybrid nature of Storm Poly.

Drawing a firm conclusion from these diagrams is challenging because they only cover a 24-hour period, while the definitions of (sub-)tropical cyclones require this structure to be visible for at least 36 hours, which is approximately the entire lifespan of Storm Poly. Moreover, warm seclusions are indistinguishable from subtropical systems in phase space diagrams (Dekker et al., 2018). And of course, one does not exclude the other. SCs can be formed through warm seclusion development and they are characterized by their thermal hybrid structure. (Quitián-Hernández et al., 2020). There are quite strong indications that the hybrid period or ST was interrupted by Poly making landfall, severing its connection with warm seawater. While a SJ-like phenomenon may have contributed, the clear presence of convection and the abrupt cessation of Poly's intensification suggest otherwise.

Ultimately, the meteorologists are intrigued by our hypothesis that a subtropical mechanism might have been involved. This explanation accounts for all the perplexing aspects of Storm Poly: the rapid intensification, the location of the wind, the sudden deviation from the predicted track, the apparent presence of two centres and the high wind intensity. In hindsight, the development of Poly itself is not particularly unusual, but its occurrence in this specific location makes it unique. As far as we know, we have never seen a cyclone undergoing ST over the North Sea before. Which is why Dutch meteorologists are not familiar with the occurrence of subtropical-like systems in this region. Studies on the phase transitions between TCs, SCs, and ETCs highlight this as a characteristic of SCs. Identifying SCs poses challenges for forecasters as they exhibit a range of baroclinic and convective structures, varying between more extratropical and more tropical characteristics (Quitián-Hernández et al., 2020; Wood et al., 2023).

Another factor that introduces uncertainties in this research is the assumption that SST changes uniformly. This assumption is not entirely realistic, as observations indicate that the Channel and coastal regions experience more significant temperature increases compared to the middle of the North Sea. Similarly, the

Bay of Biscay warms more than the surrounding ocean (Huang et al., 2021). These temperature variations contribute to greater regional baroclinicity, which is not investigated in this study.

Recommendations for further research

Firstly, we need to investigate past severe summer storms in the Netherlands to determine whether Storm Poly is the first of its kind with hybrid characteristics in the region. The top-10 list of significant summer storms from KNMI includes storms occurring in May and September, categorized based on their timing rather than their nature. Potential candidates for further investigation are the storms that occurred on 28 May 2000, 13 September 2017, 25 July 2015, and 14 August 1985, ranked 1, 3, 5, and 6 respectively, if we consider late May and early September as true summer storms. We cannot yet conclusively state from this list that Storm Poly is the first hybrid storm to form over the North Sea or to initiate ST in this region. At first glance, the storm tracks of storms ranked 1 and 5 on the list appear quite similar in location and timing. Storm 5 also formed off the coast of Brittany and moved through the Channel into the North Sea. Despite being ranked higher than Storm Poly, this storm had a maximum hourly average wind speed of 10 Bft and peak gusts of 122 km/h. The strongest summer storm, ranked 1, also reached 'only' 10 Bft with maximum gusts of 130 km/h. Poly had an hourly average windspeed of 11 Bft for two consequtive hours and a maximum recorded windgust of 146 km/h! While these storms impacted larger areas, it highlights how exceptionally strong Storm Poly was, even if only locally. The question remains: how exceptional was it really, and can we expect more of such storms in the future with climate change?

Secondly, the implications for future KNMI climate scenarios. While there has been extensive research on TCs undergoing ET and affecting Europe, there are not many studies on the formation of hybrid storms north of 40 degrees latitude. The KNMI climate scenarios mainly focus on the increase in autumn storms and the potential migration of former tropical systems to Europe, but not on the possibility of convective storms like Poly forming over the North Sea (KNMI, 2023). If such hybrid storm systems become more frequent, it is crucial to prepare our meteorologists for these scenarios, as they are unpredictable and can cause significant damage. Was Storm Poly a 'freak' event or a preview of the future? Our suggestion is to analyze individual storms in future climate model runs to investigate factors like latent heating, vertical wind shear, upper and low-level disturbances in these storms and identify their key characteristics and possible impacts as they vary between different cyclone types (Wood et al., 2023). Understanding this will help us better prepare for and mitigate the impacts of such hybrid storms in the future.

Another recommendation from our RACMO dSST experiment is to adjust the SST anomaly instead of using a uniform SST field as had been previously done by Bui and Spengler (2021). This approach would allow for a more accurate investigation of the influence of SST on baroclinicity and how it might affect future storms over the North Sea.

4 Conclusions

In this study, we investigate the development and intensification of Storm Poly, a significant summer windstorm, by analyzing the interaction between atmospheric systems and the influence of sea surface temperatures (SSTs). We utilize high-resolution datasets such as the ERA5 and the new cycly of HARMONIE (CY46) to examine the storm's evolution. With the Regional Atmospheric Climate Model (RACMO), we conduct Pseudo Global Warming (PGW) simulations, which unfortunately do not yield useful results due to limitations in initial conditions and spin-up time. To address this, we design a new experiment involving a uniform SST perturbation (RACMO dSST). This approach allows us to isolate the impact of SST on Storm Poly's development more effectively, providing clearer insights into the role of SST anomalies in the storm's behavior. Additionally, the study explores the hypothesis of a sting-jet (SJ) phenomenon contributing to Poly's severe wind gusts.

Storm Poly's development was a direct consequence of the interaction between an upper-level trough and a cluster of convective showers. This interaction is exemplified by a significant upper-level potential vorticity (PV) anomaly aligning with a low-level disturbance, as captured in both the ERA5 and CY46 datasets. The rapid intensification phase of Storm Poly was a result of the merging of these systems. The analysis reveals the presence of two distinct convective systems at the lower levels that eventually coalesced into a single, more powerful cyclone, indicating a complex interaction similar to the Fujiwhara effect, wherein the interplay between multiple vortices significantly influences the storm's trajectory and strength. ERA5 reanalysis data, while providing a broad overview of the atmospheric conditions, struggles with precise temporal and intensity estimations of wind during Poly's peak. This discrepancy underscores the limitations of ERA5's resolution in capturing extreme weather events with fine spatial and temporal detail. In contrast, the higher resolution CY46 dataset depicted a more nuanced picture. It identified the formation of a low-level wind maximum formed just south of the low-level positive PV anomaly, which coincided with the region of the highest wind speeds recorded and a SJ was suspected. Further investigation into the SJ hypothesis, commonly associated with severe windstorms, reveals that this was not the cause of the strong surface winds in Storm Poly. Instead, the strongest winds are consistently observed at the surface level, implying that surface processes rather than mid-level descending jets were primarily responsible for the observed wind extremes. This low level wind maximum, characterized by intensified zonal winds and significant convective activity, suggests that the lower atmosphere's dynamics were crucial in generating the extreme surface winds observed during Storm Poly. The convective zones identified in CY46, particularly on the southern side of the storm's core, revealed the importance of latent heat release and warm-core processes in driving Poly's strength.

The RACMO PGW simulations provide some additional insights, albeit with notable limitations due to initial condition inaccuracies and insufficient spin-up time. Analysis of the RACMO HindCast results reveals that the presence of a cluster of showers over Brittany significantly affects the initial conditions, thereby influencing the storm's evolution. Despite these limitations, the PGW simulations indicate that a track over land tends to weaken the storm, whereas a path over the North Sea increases its intensity. This finding underscores the importance of accurate initial conditions and appropriate spin-up times for reliable storm predictions in PGW climate simulations. Our RACMO dSST simulations suggest that while the SST of the North Sea did influence the storm, it was not the primary mechanism behind its rapid intensification. Instead, the interaction between the storm and the low-level disturbance plays a more significant role. Lower SSTs result in a higher minimum MSLP and an earlier end to the rapid intensification phase. Conversely, higher SSTs are associated with increased maximum wind speeds, greater precipitation, and a larger impact area. Despite these influences, the lowest MSLP values across all scenarios remain close to 988 hPa, with no substantial decrease for higher SST runs compared to the control. We suggest that this is because the connection of Poly to the sea water was cut short by its early landfall, preventing further deepening. All scenarios also contain the bombogenesis of Storm Poly, while the same simulation at earlier initiation do not contain this effect. This suggests that while SST variations did impact the storm's characteristics, they were not the dominant factor driving Poly's rapid intensification. The rapid intensification and presence of a warm-core were the result of these convective showers. The findings do suggest that warmer conditions, through increased SSTs and the frequency of convective events, may exacerbate the challenges in forecasting similar storms in the future.

The geopotential thickness diagrams reveal a shallow warm-core at the surface and a cold-core in the upper levels. They also show that the higher SST runs enhance warm-core dynamics and promote deeper convection. Storm Poly appeared to be primarily driven by large-scale dynamics, where lower SSTs would likely have resulted in less intense (or absent) warm-core dynamics. Moreover, the phase space diagram analysis initially shows an asymmetric cold-core cyclone that develops a shallow warm-core with increasing symmetry. This confirms that Storm Poly exhibited characteristics of a hybrid cyclone that initiated subtropical transition over the North Sea but failed to complete it due to early landfall.

In conclusion, while SST variations influence the intensity and dynamics of Storm Poly, the development and intensification rate of Storm Poly seems mostly driven by the interaction of different atmospheric systems. The SST of the North Sea played a supportive but not dominant role in the storm's evolution. Additionally, Storm Poly can be classified as a hybrid cyclone that started subtropical transition over the North Sea. This finding underscores the complexity of storm dynamics and the necessity of considering multiple factors, including atmospheric interactions, latent heating processes, and transitional characteristics, in understanding and predicting future storm behavior in a changing climate.

References

Berg, R. (2021). Subtropical Storm Alpha. *National Hurricane Center*.

Brand, S., & Guard, C. (1978). Extratropical Storm Evolution from Tropical Cyclones in the Western North Pacific Ocean:. *Defense Technical Information Center*. https://doi.org/DOI:10.21236/ADA060910

Brogli, R., Heim, C., Mensch, J., Sørland, S., & Schär, C. (2023). The pseudo-global-warming (PGW) approach: methodology, software package PGW4ERA5 v1.1, validation, and sensitivity analyses. *Geoscientific Model Development*, *16*(3), 907–926. https://doi.org/10.5194/gmd-16-907-2023

Browning, K. (2004). The sting at the end of the tail: damaging winds associated with extratropical cyclones. *Quarterly Journal of the Royal Meteorological Society*, *130*(597), 375–399. https://doi.org/10.1256/qj.02.143

Bui, H., & Spengler, T. (2021). On the Influence of Sea Surface Temperature Distributions on the Development of Extratropical Cyclones. *Journal of the Atmospheric Sciences*, *78*(4), 1173–1188. https://doi.org/10.1175/JAS-D-20-0137.1

Clark, P., & Gray, S. (2018). Sting jets in extratropical cyclones: a review. *Quarterly Journal of the Royal Meteorological Society*, *144*(713), 943–969. https://doi.org/10.1002/qj.3267

de Vries, H., Scher, S., Haarsma, R., Drijfhout, S., & van Delden, A. (2019). How Gulf-Stream SST-fronts influence Atlantic winter storms. *Climate Dynamics*, *52*(1), 5899–5909. https://doi.org/10.1007/s00382-018-4486-7

Dekker, M., Haarsma, R., de Vries, H., Baatsen, M., & van Delden, A. (2018). Characteristics and development of European cyclones with tropical origin in reanalysis data. *Climate Dynamics*, *50*(1), 445–455. https://doi.org/10.1007/s00382-017-3619-8

Evans, J., & Braun, A. (2012). A Climatology of Subtropical Cyclones in the South Atlantic. *Journal of Climate*, *25*(21), 7328–7340. https://doi.org/10.1175/JCLI-D-11-00212.1

Evans, J., & Hart, R. (2003). Objective Indicators of the Life Cycle Evolution of Extratropical Transition for Atlantic Tropical Cyclones. *Monthly Weather Review*, *131*(5), 909–925. https://doi.org/10.1175/1520-0493(2003)131⟨0909:OIOTLC⟩2.0.CO;2

Fujiwhara, S. (1921). The natural tendency towards symmetry of motion and its application as a principle in meteorology. *Quarterly Journal of the Royal Meteorological Society*, *47*(200), 287–292. https://doi.org/10.1002/qj.49704720010

Gozzo, L., Rocha, R., Reboita, M., & Sugahara, S. (2014). Subtropical Cyclones over the Southwestern South Atlantic: Climatological Aspects and Case Study. *Journal of Climate*, *27*, 8543–8562. https://doi.org/10.1175/JCLI-D-14-00149.1

Guishard, M., Evans, J., & Hart, R. (2009). Atlantic Subtropical Storms. Part II: Climatology. *Journal of Climate*, *22*(13), 3574–3594. https://doi.org/10.1175/2008JCLI2346.1

Hart, R. (2003). A Cyclone Phase Space Derived from Thermal Wind and Thermal Asymmetry. *Monthly Weather Review*, *131*(4), 585–616. https://doi.org/10.1175/1520-0493(2003)131⟨0585:ACPSDF⟩2.0.CO;2

Hersbach, H., Bell, B., Berrisford, P., & Hirahara, e. a., S. (2020). The ERA5 global reanalysis. *Quarterly Journal of the Royal Meteorological Society*, *146*(730), 1999–2049. https://doi.org/10.1002/qj.3803

Huang, B., Liu, C., Banzon, V., Freeman, E., Graham, G., Hankins, B., Smith, T., & Zhang, H. (2021). Improvements of the Daily Optimum Interpolation Sea Surface Temperature (DOISST) Version 2.1. *Journal of Climate*, *34*(8), 2923–2939. https://doi.org/10.1175/JCLI-D-20-0166.1

KNMI. (2023). KNMI'23-klimaatscenario's voor Nederland. *KNMI, De Bilt*. https://doi.org/KNMI-Publicatie23-03

Kornegay, F., & Vincent, D. (1976). Kinetic Energy Budget Analysis During Interaction of Tropical Storm Candy (1968) with an Extratropical Frontal System. *Monthly Weather Review*, *104*(7), 849–859. https://doi.org/https://doi-org.proxy.library.uu.nl/10.1175/1520-0493(1976)104⟨0849:KEBADI⟩2.0.CO;2

Manning, E., Kendon, E., Fowler, H., & Roberts, M. (2023). Projected increase in windstorm severity and contribution from sting jets over the UK and Ireland. *Weather and Climate Extremes*, *40*(100562), 0. https://doi.org/10.1016/j.wace.2023.100562

Manning, E., Kendon, E., Fowler, H., Roberts, N., Berthou, S., Suri, D., & Roberts, M. (2022). Extreme windstorms and sting jets in convection-permitting climate simulations over Europe. *Climate Dynamics*, *58*(9), 2387–2404. https://doi.org/10.1007/s00382-021-06011-4

Quitián-Hernández, L., González-Alemán, J., Santos-Muñoz, D., Fernández-González, S., Valero, F., & Martín, M. (2020). Subtropical Cyclone Formation via Warm Seclusion Development: The Importance of Surface Fluxes. *Journal of Geophysical Research: Atmospheres*, *125*(8), e2019JD031526. https://doi.org/10.1029/2019JD031526

Reboita, M., Gozzo, L., Crespo, N., Custodio, M., Lucyrio, V., de Jesus, E., & da Rocha, R. (2022). From a Shapiro–Keyser extratropical cyclone to the subtropical cyclone Raoni: An unusual winter synoptic situation over the South Atlantic Ocean. *Quarterly Journal of the Royal Meteorological Society*, *148*(747), 2991–3009. https://doi.org/10.1002/qj.4349

Schär, C., Frei, C., Lüthi, D., & Davies, H. (1996). Surrogate climate-change scenarios for regional climate models. *Geophysical Research Letters*, *23*(6), 669–672. https://doi.org/10.1029/96GL00265

Seneviratne, S., Zhang, X., Adnan, M., Badi, W., Dereczynski, C., Di Luca, A., Ghosh, S., Iskandar, I., Kossin, J., Lewis, S., Otto, F., Pinto, I., Satoh, M., Vicente-Serrano, S., Wehner, M., & Zhou, B. (2021). Weather and Climate Extreme Events in a Changing Climate. *Climate Change 2021: The Physical Science Basis. Contribution of Working Group I to the Sixth Assessment Report of the Intergovernmental Panel on Climate Change[Masson-Delmotte, V., P. Zhai, A. Pirani, S.L. Connors, C. Péan, S. Berger, N. Caud, Y. Chen, L. Goldfarb, M.I. Gomis, M. Huang, K. Leitzell, E. Lonnoy, J.B.R. Matthews, T.K. Maycock, T. Waterfield, O. Yelekçi, R. Yu, and B. Zhou (eds.)]*, *Cambridge University Press*, 1513–1766. https://doi.org/10.1017/9781009157896.013

Shapiro, M., & Keyser, D. (1990). Fronts, jet streams, and the tropopause. *Newton CW, Holopainen EO (eds) Extratropical Cyclones, the Erik Palmén memorial volume*(Am Meteorol Soc, Boston), 167–191.

Sinclair, V., Rantanen, M., Haapanala, P., Räisänen, J., & Järvinen, H. (2020). The characteristics and structure of extra-tropical cyclones in a warmer climate. *Weather and Climate Dynamics*, *1*(1), 1–25. https://doi.org/10.5194/wcd-1-1-2020

Studholme, J., Fedorov, A., Gulev, S., Emanuel, K., & Hodges, K. (2022). Poleward expansion of tropical cyclone latitudes in warming climates. *Nature Geoscience*, *15*(1), 14–28. https://doi.org/10.1038/s41561-021-00859-1

Studholme, J., Hodges, K., & Brierly, C. (2015). Objective determination of the extratropical transition of tropical cyclones in the Northern Hemisphere. *Tellus A*, *67*. https://doi.org/10.3402/tellusa.v67.24474

Tamarin-Brodsky, T., & Kaspi, Y. (2017). Enhanced poleward propagation of storms under climate change. *Nature Geoscience*, *10*(12), 908–913. https://doi.org/10.1038/s41561-017-0001-8

Varlas, G., Pytharoulis, L., Steeneveld, G.-J., Katsafados, P., & Papadopoul, A. (2023). Investigating the impact of sea surface temperature on the development of the Mediterranean tropical-like cyclone "Ianos" in 2020. *Atmospheric Research*, *291*, 106827. https://doi.org/10.1016/j.atmosres.2023.106827

Wood, K., Yanase, W., Beven, J., Camargo, S., Courtney, J., Fogarty, C., Fukuda, J., Kitabatake, N., Kucas, M., McTaggart-Cowan, R., Reboita, M., & Riboldi, J. (2023). Phase transitions between tropical, subtropical, and extratropical cyclones: A review from IWTC-10. *Tropical Cyclone Research and Review*, *12*(4), 294–308. https://doi.org/10.1016/j.tcrr.2023.11.002

Wu, Y., Ting, M., Seager, R., Huang, H., & Cane, M. (2011). Changes in storm tracks and energy transports in a warmer climate simulated by the GFDL CM2.1 model. *Climate Dynamics*, *37*(1), 53–72. https://doi.org/10.1007/s00382-010-0776-4

Zarzycki, C., Thatcher, D., & Jablonowski, C. (2017). Objective tropical cyclone extratropical transition detection in high-resolution reanalysis and climate model data. *Journal of Advances in Modeling Earth Systems*, *9*(1), 130–148. https://doi.org/10.1002/2016MS000775

5 Appendix

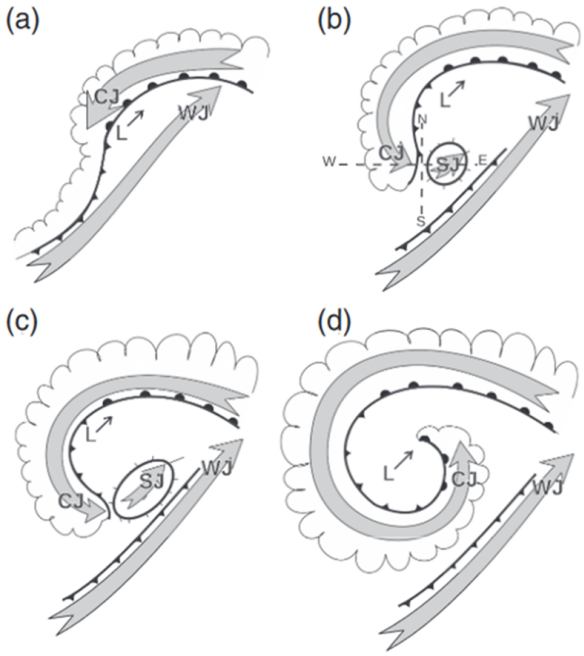

Figure 23: Conceptual model of the near-surface flows in an ETC. (a) Early stage of frontal wave cyclone development. L denotes low-pressure centre with direction of movement shown by the thin arrow. Grey arrows show the system-relative low-level jets; WJ is the warm-conveyor-belt jet (WCB in text) and CJ the cold conveyor- belt jet (CCB in text). (b) frontal-fracture phase, when the SJ first appears at the surface. (c) As the cloud head wraps round further, the SJ region extends. (d) Eventually the distinct SJ disappears and the dominant low-level wind in this region is due to the CJ. Positions of cross-sections shown in Figure 6 are marked in (b). Used with permission from Clark et al. (2005). From Clark and Gray (2018).

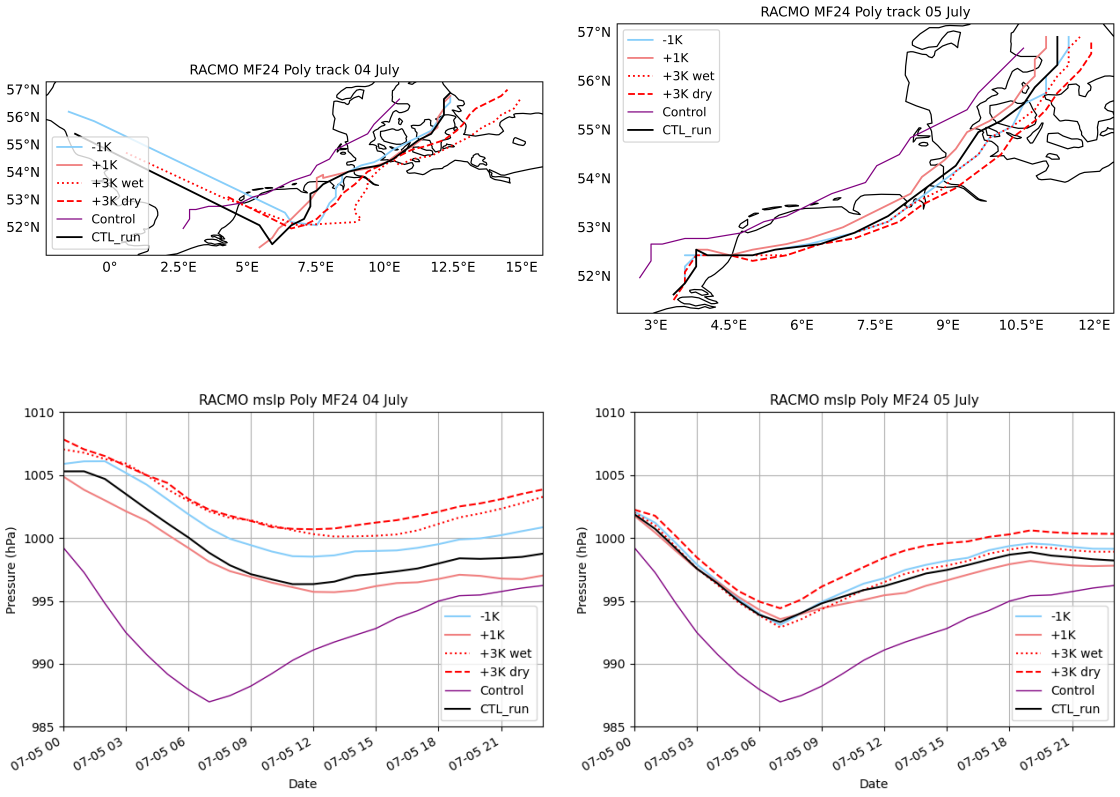

(a) (b)

Figure 24: Storm track and MSLP of Storm Poly in RACMO's PGW simulations. Left: Simulation initiated on July 4 at 0000 UTC, using the 24 hour forecast. Right: Simulation initiated on July 5 at 0000 UTC, using the 24 hour forecast. Top panels: Storm track of Poly, determined by minimum MSLP, from July 5 at 0000 UTC to July 5 at 2300 UTC. Bottom panels: Minimum MSLP of Poly during the same period

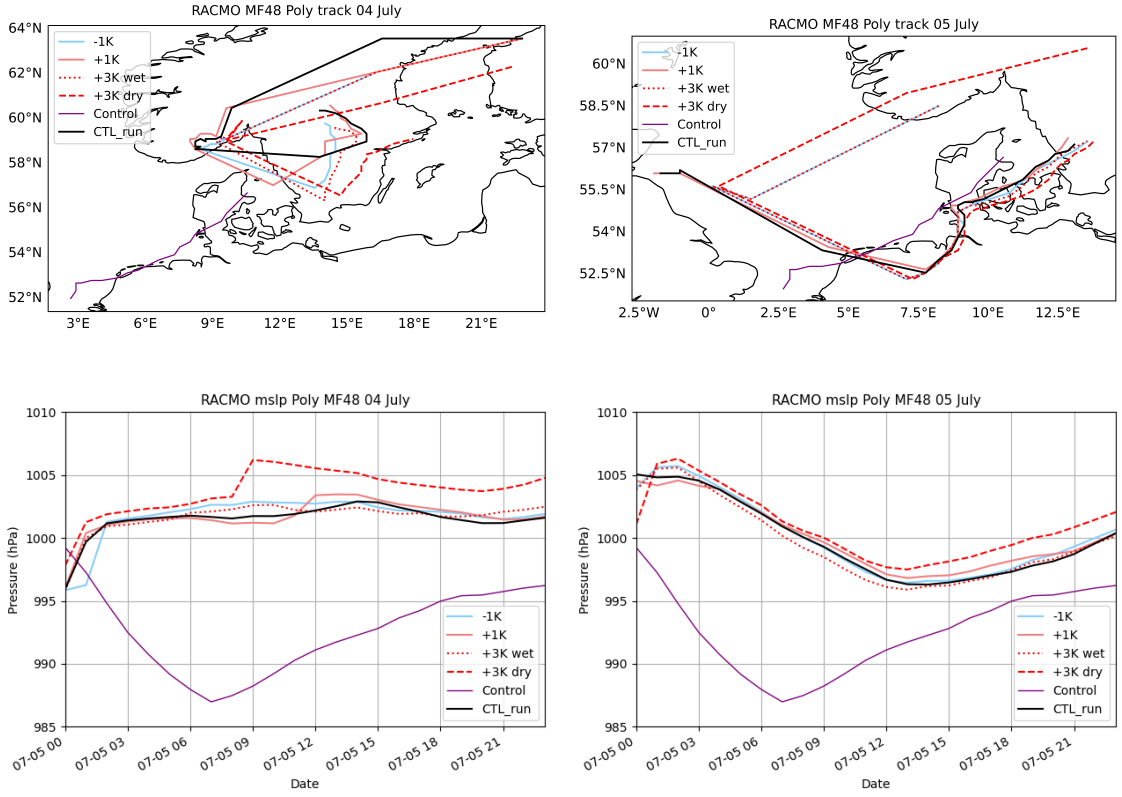

(a) (b)

Figure 25: Storm track and MSLP of Storm Poly in RACMO's PGW simulations. Left: Simulation initiated on July 4 at 0000 UTC, using the 48 hour forecast. Right: Simulation initiated on July 5 at 0000 UTC, using the 48 hour forecast. Top panels: Storm track of Poly, determined by minimum MSLP, from July 5 at 0000 UTC to July 5 at 2300 UTC. Bottom panels: Minimum MSLP of Poly during the same period

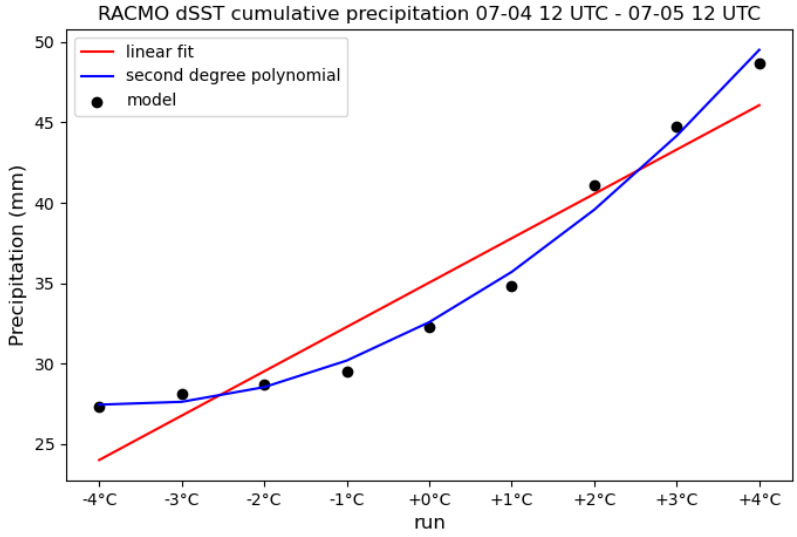

Figure 26: Linear and second-order polynomial fit of the total 24-hour precipitation in the grid cell marked by a yellow star in Fig.18b, showing an exponential increase in precipitation.

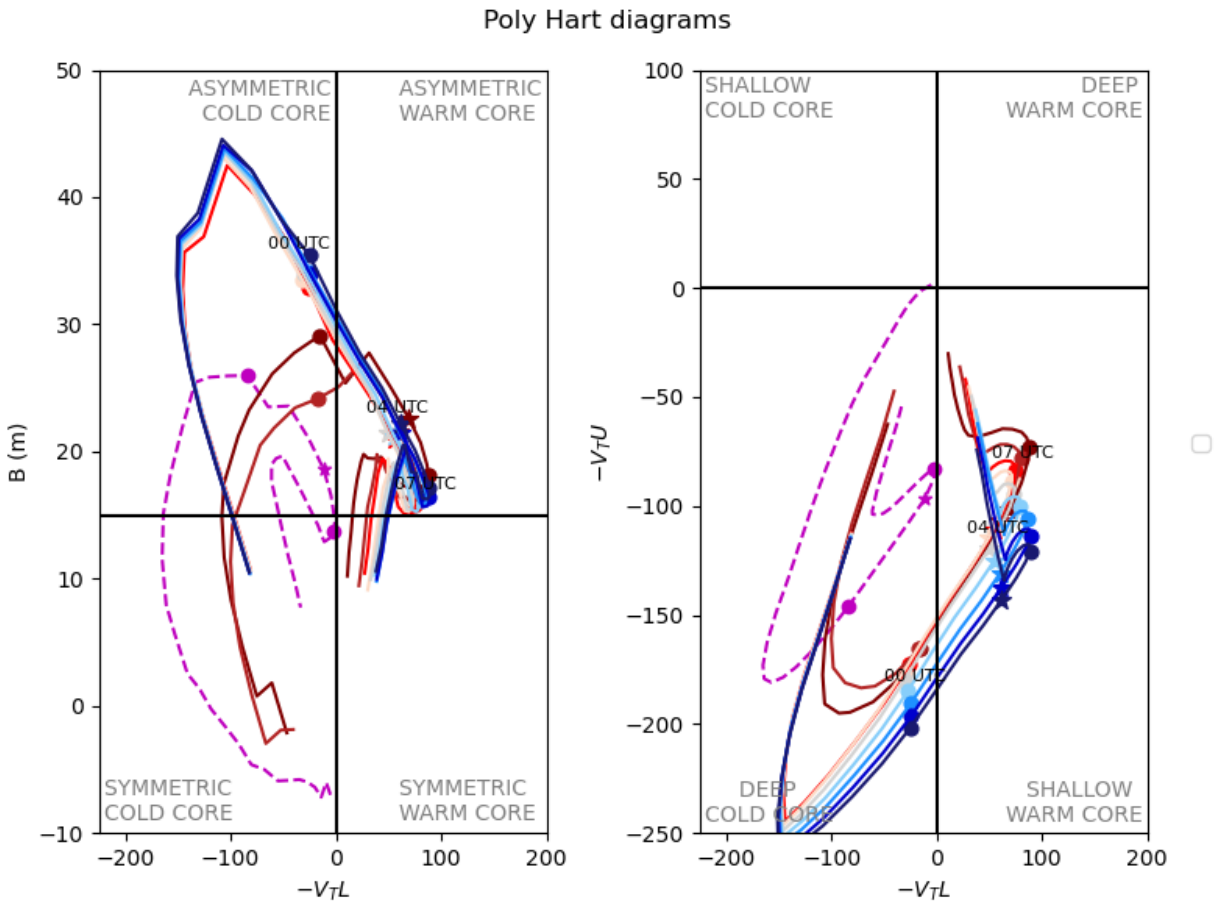

Figure 27: Phase space (Hart-) diagram of Storm Poly using ERA5 data and RACMO dSST data. Upper-level is 700 hPa-400 hPa, lower-level is 1000 hPa - 700 hPa

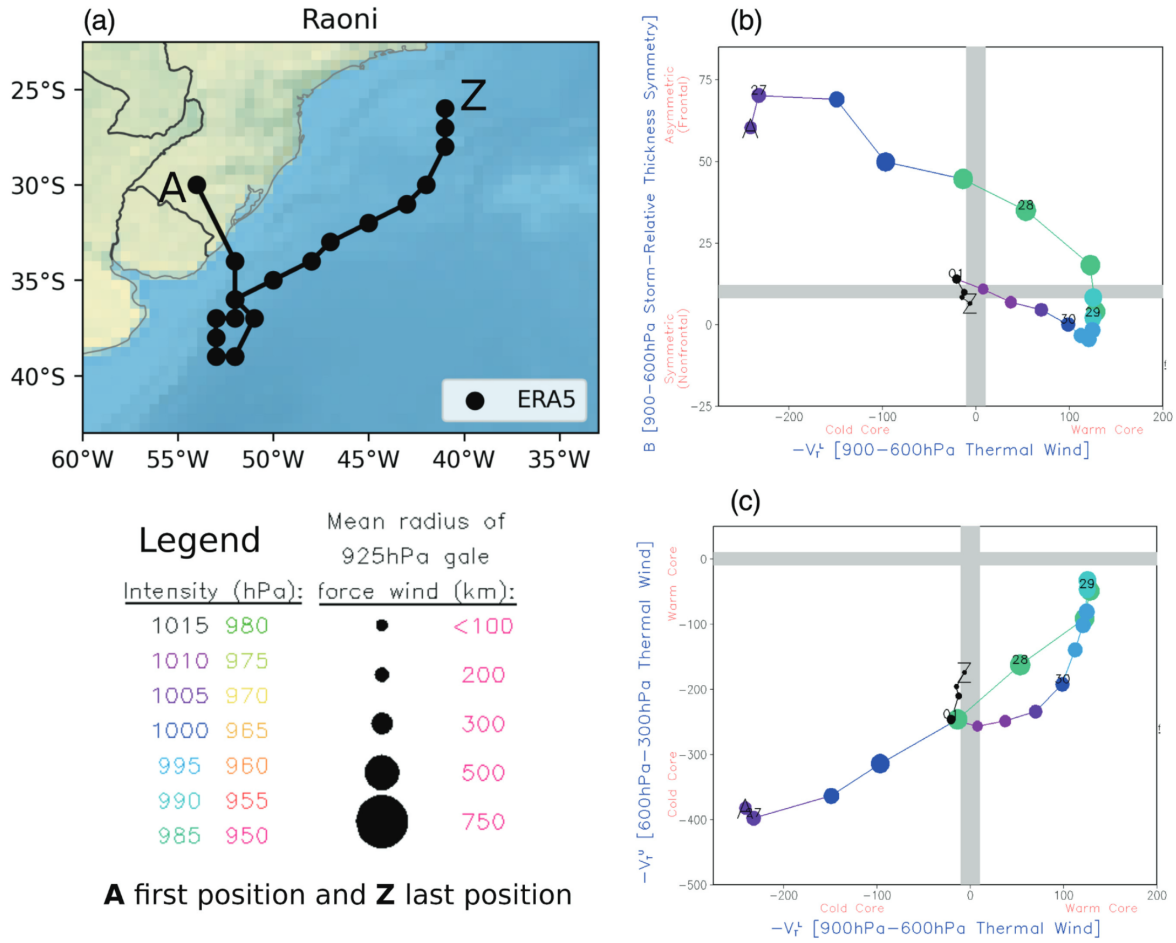

Figure 28: (a) ERA5 cyclone track (lines and dots) at every 6 hr from genesis (1800 UTC 26 June) to lysis (1800 UTC 1 July). Cyclone phase space (CPS) parameters at each 6 hr: (b) B versus V_T^L and (c) V_T^L versus V_T^U . A and Z indicate, respectively, cyclogenesis and cyclolysis. The legend below (a) indicates the mean radius of gale-force winds at 925 hPa (threshold is 17 m s^1) in circles with different sizes and MSLP (hPa) in colours (Colour figure can be viewed at wileyonlinelibrary.com). From Reboita et al. (2022)